THESIS

CARBON-ION RADIATION BIOLOGICAL LETHAL DOSE DISTRIBUTION

Submitted by

Dylan Buglewicz

Department of Environmental and Radiological Health Sciences

In partial fulfillment of the requirements

For the Degree of Master of Science

Colorado State University

Fort Collins, Colorado

Summer 2018

Master's Committee:

Advisor: Takamitsu Kato

Marie Legare
Aaron Sholders

ABSTRACT

CARBON-ION RADIATION BIOLOGICAL LETHAL DOSE DISTRIBUTION

Background: Carbon-ion radiotherapy is an emerging modality used in cancer therapy. It has been very successful in treating solid cancers due to its excellent physical dose-distribution and deposition around the carbon-ion beam Bragg peak. Furthermore, its high-LET components allow for the treatment of tumors displaying radioresistance to low-LET radiotherapy modalities.

Purpose: This present study was designed to investigate the biological range in which the carbon-ion beam irradiation distributes dosages resulting in significant cell death and how increases in initial dosage may impact this range. Furthermore, we sought to investigate how carbon-ion irradiation-induced genotoxicity may correlate with this biological range.

Methods: Cellular lethality or genotoxicity via cell survival assays or cytokinesis-block micronucleus assays (CBMN), respectively, of monoenergetic 290 MeV/n carbon-ion beam irradiation were compared at increasing depths of CHO treated cells cultured in T-175 flasks. Cells were irradiated with initial dosages of either 1, 2 or 3 Gy for cell survival assays or an initial dosage of 1 Gy for CBMN assays. Following irradiation, cells were evaluated through survival fractions or micronuclei formation at specific depths, depending on the system.

Results: Under all irradiation initial dosages of monoenergetic 290 MeV/n carbon-ion beams, survival fraction decreased as depth increased up to 14.5 cm. This depth was defined as our biologically observed Bragg peak due to there being few to no observable colonies. Following this depth there was a rapid increase in survival fraction at 15.0 cm. We observed survival fractions were most significantly reduced for the initial dosages of 1, 2 or 3 Gy between

the ranges of 14.0 – 14.5, 13.5 – 14.5 and 12.5 – 14.5 cm ($P < 0.0001$), as well as, reappearance of colony formation occurring at the depths of 14.72, 14.77 and 14.78 cm, respectively. Micronuclei formation coincided with our cell survival assays treated with 1 Gy initial dosage, as micronuclei frequency increased as the depth increased up to 14.5 cm, indicative of an increased genotoxicity up to this depth.

Conclusion: Monoenergetic 290 MeV/n carbon-ion beams with 1, 2 or 3 Gy initial dosages displayed a biologically observed Bragg peak at the depth of 14.5 cm and portrayed a biological lethal dose range of 0.72, 1.27 and 2.28 cm, respectively.

Future Directions: Compare results obtained in this study with the clinically applicable carbon-ion spread-out Bragg peak (SOBP) technique to decipher if this technique induces the same cellular lethality. Compare results obtained in this study with the proton beam to decipher the degree in which the carbon-ion beam better distributes its lethal dosage. Enhance the efficiency in which the carbon-ion induces cell death via treatment of cells with a radiosensitizer.

ACKNOWLEDGEMENTS

I would like to thank my advisor Dr. Takamitsu Kato whose kindness and guidance has had a tremendous impact on my development as a researcher and as a person. His genuine passion for research as well as providing me with the opportunity to travel across the world has heightened my desire to further pursue research as a profession. Dr. Kato goes far beyond expectations as an advisor and our time together has led me to consider him as a dear friend. Working with Dr. Kato has helped me realize that I can make a difference in this world through my research and my potential for helping others is limitless.

I would also like to thank my committee members Dr. Aaron Sholders and Dr. Marie Legare. Words alone cannot explain my tremendous gratitude and appreciation for Dr. Sholders. He is not only a great professor but a great person as well who has always been there for me. It has been a true blessing to have had the opportunity to get to know him over these past years. Dr. Legare's passion for science is not only inspiring but is also contagious. Her kindness and willingness to help speaks volumes on how wonderful of a person she is.

I would like to also thank everyone who made this research possible. I would like to thank JAXA for funding my travels and research in Japan. A special thank you to Dr. Fujimori at NIRS for allowing us to use his laboratory while in Japan and always being more than willing to lend a helping hand. I would like to thank Austin Banks for all his hard work and contribution with generation of our surface plots.

TABLE OF CONTENTS

LIST OF TABLES

LIST OF FIGURES

CHAPTER ONE

BACKGROUND

1.1 Introduction

"You have cancer," the three words which bring your mortality up close and personal, the daunting realization your time on earth may be running out. As cancer remains the leading cause of death globally [1] and about 1.7 million new cancer cases are expected to be diagnosed in the U.S. in 2018 [2], improvements in cancer therapies are critical to save lives and differentiate the diagnosis of cancer from the death sentence it once was. Today there are three main cancer treatment modalities; surgery, chemotherapy and radiotherapy [3]. With the varying types, sizes, and location of differing cancers, each modality may best be used alone or in conjunction with the others. Another contributing factor for which treatment modality to utilize comes with its financial cost vs treatment effectiveness. This can place a financial strain on the best treatment options, particularly in developing countries. According to the Agency for Health Care Research and Quality, in the U.S. in 2015 there was about $80.2 billion in the U.S. on cancer-related healthcare [2].

However, technological advancements in ionizing radiation over the past few decades have greatly reduced the cost of undergoing radiotherapy and have improved the accuracy at which the dose can be distributed to the tumor. Therefore, allowing for a more precise deposition of dose into the target tumor, while reducing damage in the normal surrounding tissue and enabling radiotherapy to become one of the most effective treatment modalities utilized for a wide variety of cancer types [4].

1.2 Three Main Cancer Treatment Modalities

Surgery is the direct approach in removing cancerous tumors, diagnose cancer, or can even be used to address the extent of which the cancer has spread. However, it is highly invasive and is typically the less preferred option when dealing with tumors close in proximity to delicate organs, such as the brain. Surgery may also be dangerous to elderly patients, as the recovery time may be too strenuous for these individuals. Furthermore, patients undergoing surgery may incur many financial charges as it can involve multiple medical providers, hospitals, specialized facilities, etc. [5].

Another cancer treatment modality is chemotherapy, which utilizes certain medications to stop or slow the growth of cancerous cells. These medications attack rapidly growing cancerous cells. However, they may also attack rapidly growing non-cancerous cells, resulting in a variety of unwanted side-effects. In a previous study examining side-effects of 99 patients undergoing chemotherapy they found that 54% of the patients endured 15 of the most severe symptoms involving non-physical side-effects and a majority of the patients suffered from the major physical side-effects, such as vomiting, nausea and hair loss [6]. While these side-effects can be detrimental to the patient's health, a major area of concern involves chemotherapies cardiac side-effects. Prior studies have also revealed that chemotherapy may result in cardiovascular and/or coronary artery disease, particularly in older patients [7, 8]. As such, the decision to treat cancer with chemotherapy involves weighing the benefits of its anti-tumor effects vs the side-effects it may induce.

The most notable and expanding cancer treatment modality is radiotherapy. It has become an important component of cancer treatment with approximately 50% of cancer patients undergoing radiation therapy and contributing towards 40% of curative treatments for cancer [9].

This modality has been very successfully used for treating solid cancers that would otherwise be difficult to remove via an invasive surgical procedure that may not fully eradicate malignant tumors, such as in the head and neck [10, 11].

Radiotherapy follows its fundamental principle to deliver a precise dose of radiation to the target tumor tissue while minimizing radiation/damage to the surrounding healthy tissue, thus limiting any unwanted side-effects [12]. This principle plays an important role when treating bone tumors, particularly chordomas, as they are highly responsive to carbon-ion radiotherapy and allows for the maximum preservation of the adjacent organs, as well as their functions, which would be difficult to accomplish via an invasive surgery. Radiotherapy can also be used either before surgery (neoadjuvant therapy) to shrink the tumor, or it can be utilized after surgery (adjuvant therapy) to destroy any remaining tumor cells [9]. Although, the disadvantage to radiotherapy is that it utilizes complex equipment, specialized facilities, a team of health care providers and patients may be required to receive several radiation treatments over several weeks, which all contributes to an increased financial cost and thus has limited these facilities to more economically advanced countries [5]. Furthermore, radiotherapy selectively targets tumors which means it is not helpful in treating cancers that have spread to many places within the body, i.e. metastasized.

1.3 General Radiobiology

The main goal behind radiotherapy is to deprive cancer cells of their reproductive potential [13]. Radiation-induced damage to cells results from DNA damages in the form of single stranded DNA breaks (SSBs), double stranded DNA breaks (DSBs), base damage, or their combinations [14, 15]. Among these DNA damages, DSBs are considered the major actor for

inducing cell death. If these DSBs are left unrepaired or are improperly repaired, they may lead to human disorders including cancer [16]. When radiation-induced DNA damage is extensive and cell-cycle check-point functions are impaired, as often found in tumor cells, unrepaired DNA can pass through these check points and can result in significant chromosomal aberrations during the mitotic phase [17, 18]. As a result, cells possessing DNA damage can be effectively observed by chromosomal aberrations as an indicator of radiation exposure, as these correlate well with radiation-induced cell death [19].

The cells abilities to repair DNA damage is a key aspect of radiation-induced genetic damage. In mammalian cells, induction of DSBs initiates the DNA damage response pathway involving damage recognition, information transfer, cell cycle regulation via checkpoints and the inactivation of appropriate repair systems [20, 21]. Cancer cells are often defective in certain aspects of DNA repair; however, they can possess backup pathways for accomplishing the DNA repair [4]. Moreover, cancer cells are not as efficient at repairing DNA damage even with these backup pathways, resulting in their cell death. In contrast to rapidly proliferating cancer cells, normal cells do not proliferate as quickly, which allows them to repair the damage before replication. Furthermore, radiotherapy does not kill cancer cells right away. It may take hours or even weeks of treatment before cancer cells begin to die. It may also take weeks to months for all the cancer cells in a tumor to be effectively killed off following treatment [9]. Moreover, radiation mainly kills cells either by apoptosis (programmed cell death) or mitotic catastrophe, also known as mitotic cell death [22] (Fig.1).

Mitotic catastrophe is a type of cell death that occurs during or after aberrant mitosis caused by the missegregation of chromosomes. This results in the formation of giant cells possessing multiple nuclei, otherwise known as micronuclei [23]. For solid tumors, which

radiotherapy is highly effective in treating, cell death occurs predominantly resulting from aberrant mitotic events resulting in mitotic catastrophe [24].

After radiation, there are three main biological factors of cancer cells that have shown to affect the success of radiotherapy treatment. These involve the extent of hypoxia, the ability for surviving cells to replicate/repopulate following treatment, i.e. its clonogenicity, and the intrinsic radioresistance of the cancer cells [4].

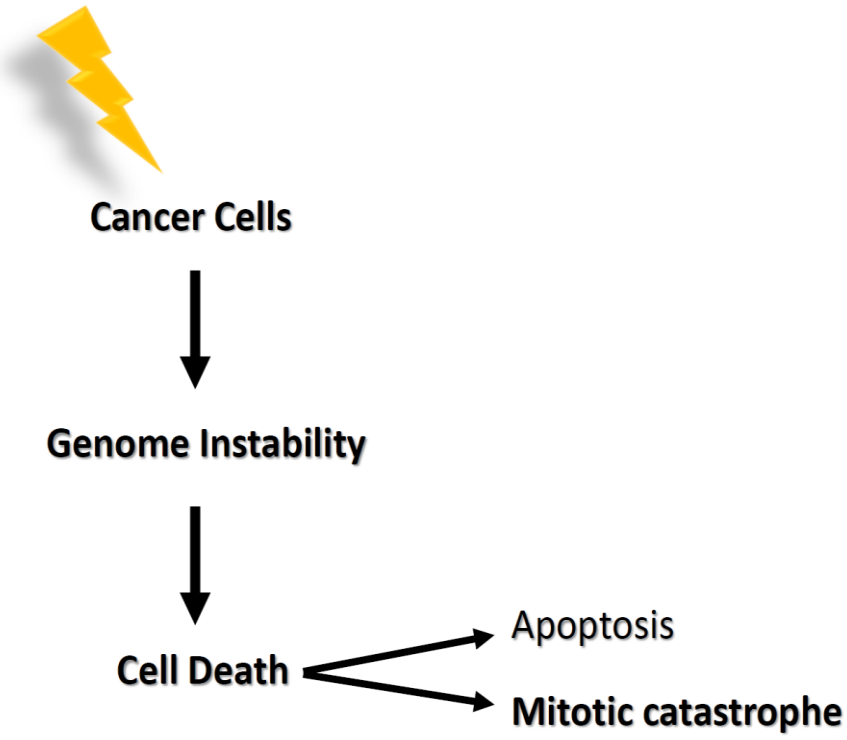

Figure 1. Radiation-induced cell death. Radiation causes genome instability and mainly kills cells either by apoptosis or mitotic catastrophe. Solid tumor cell death mainly results from mitotic catastrophe.

1.4 Linear Energy Transfer (LET) and Radiation

Linear energy transfer (LET) involves the rate at which a charged particle deposits its energy along its path, and is equivalent to the energy loss *dE/dx* which is usually measured in keV/μm [25]. Moreover, this rate increases as the mass of the particle increases [26]. Ionizing radiation can be either low-LET (sparsely ionizing) or high-LET (densely ionizing). Protons and photons are clinically considered as low-LET, while carbon-ions are considered as high-LET radiation [27].

Cell culture studies have revealed that utilization of high-LET irradiation has been far more effective than low-LET radiation for the process of cell inactivation [28, 29]. Moreover, low-LET radiations have many setbacks, discussed further below, which can limit their effectiveness of cancer treatment that high-LET radiations do not possess.

Of the various types of charged particles used in radiotherapy, protons and carbon-ions have been most widely utilized for charged particle radiotherapy. In comparison to photon beams, charged particle beams demonstrate higher cure rates with less complications. This is attributed to their precision of dose deliverance, thus limiting the dose given to normal tissues adjacent to the tumor. However, protons and heavier ions being much more massive than electrons, require bigger and more costly accelerators (cyclotrons) to produce enough kinetic energy to treat deep-seated tumors [30]. As a result, the equipment required for production of charged particle radiation is far more expensive than that for photons. Although, with technological advancements reducing the price of cyclotrons, it is likely to result in a wider use of charged particle therapy in the future [31].

Furthermore, the therapeutic value, i.e. the killing of tumor cells, of charged particle therapy is in part defined through their relative biological effectiveness (RBE). RBE is the ratio

of a given dose of charged particles at a specific depth passing through air, water, or a biological tissue relative to the dose of x-rays or gamma rays required/known to produce an equal biological effect [19]. In other words, it is the ratio of doses to reach the same level of effect when comparing two radiation modalities [32]. Generally, the heavier the particle is the larger RBE value it will have, i.e. a carbon-ion will have a larger RBE value than a proton, which in turn has a larger value than a photon [33].

$$\boldsymbol{RBE = \frac{D_{reference}}{D_{test}}}$$

1.5 Direct and Indirect Actions of Radiation

Radiation works through damaging the DNA of exposed tumor tissue leading to cell death. Radiation-induced DNA damage results from either direct and/or indirect actions (Fig.2/Fig.3). Radiation can act directly upon DNA molecules by ionizing secondary electrons produced by the incident radiation and cleaving their chemical bonds. For direct damage to occur with low-LET radiation the photon must directly "hit" the DNA molecule and with high-LET radiation the particulate can cause direct damage through electromagnetic interactions [34].

Radiation can also act indirectly as the incident radiation can produce free radicals via ionization of the surrounding water molecules (hydroxyl radical) causing DNA damage [35]. Furthermore, radiolysis of water must occur within a few molecules of DNA to cause indirect damage. Although, indirect damage is not only unique to radiation, as the hydroxyl attack from radiolysis of water is identical to that of spontaneously occurring biological events [36].

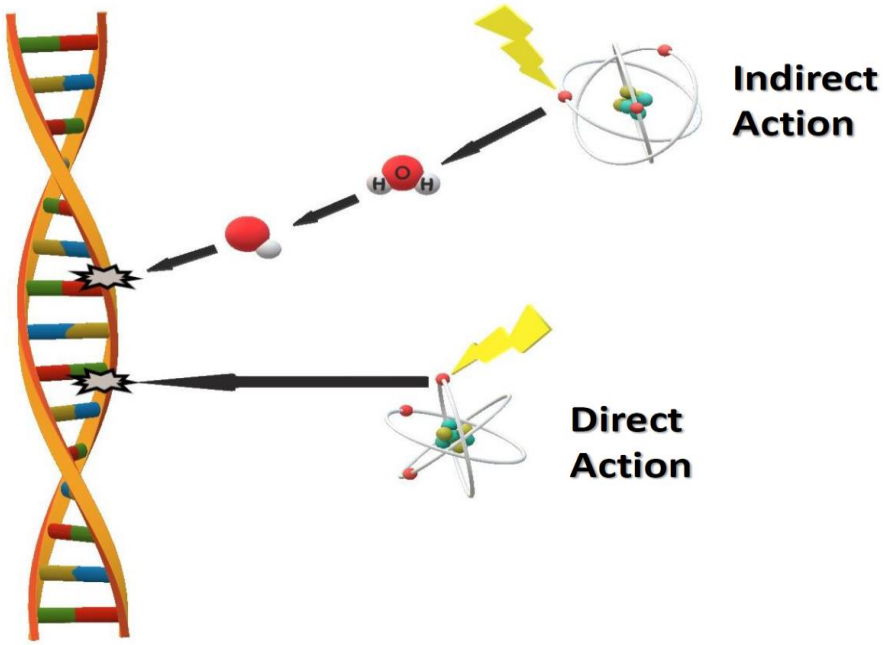

Figure 2. Radiation-induced DNA damage via indirect or direct action. Indirect action ionizes water molecules forming hydroxyl radical responsible for DNA damage. Direct action ionizes secondary electrons that directly interact with the DNA to cause damage.

Direct Action	Indirect Action
Radiation → DNA Damage → Cell Death	Radiation → Free Radicals → DNA Damage → Cell Death

Figure 3. Direct vs indirect action sequence of events leading to DNA damage and resulting in cell death. (Left) Direct action, radiation directly leads to DNA damage. (Right) Indirect action, radiation induces free radicals that cause DNA damage.

1.6 Photon Radiotherapy

X-rays and gamma rays are known as low-LET radiations, as they are composed of massless particles of energy called photons. X-rays are generated by a linear accelerator that excites electrons, while gamma rays come from the decay of substances, i.e. cobalt-60 and Cs-137 [9].

Before ionizing particle beams, there were few treatment options for treating some malignant and benign cancers. X-rays were first used to treat skin lesions a year after their discovery in 1895, even though their physical and biological characteristics were not yet fully understood. This lack in understanding lead to much morbidity and poor cancer control [37]. However, advancements in this field lead to the first successful human treatments in 1954. One such advancement included the first super-voltage x-ray tubes, built by Coolidge and became the basis of the linear accelerator, developed by Wideroe in 1927. These x-ray tubes allowed for production of orthovoltage x-rays, 200-500 kV, which were capable of treating tumors close to the surface. However, to treat deep seated tumors, more voltage was needed.

To treat tumors located in deep tissues came with the development of linear electron accelerators ("linacs") capable of producing megavoltage x-rays, 10-20 MeV, and cobalt teletherapy machines, allowing for the utilization of gamma rays as a radiotherapy modality [38]. However, these x-ray and gamma rays (cobalt) still possessed major limitations. They were observed to scatter laterally and passed beyond their targets, which made them difficult to control as they pass through tissues. As a result, they delivered high doses to large volumes of tissue [39]. These limitations made them very disappointing for use in clinical applications.

Approaches such as intensity-modulated radiotherapy (IMRT) have since increased the photon beam precision with the intent to deliver a more effective dose to the target volume while reducing the dose to tissues that do not need to be irradiated. IMRT can conform the high dose to the target volume, but the modality employs a greater number of portals and thus traverses a greater volume of normal cells [38].

1.6.1 Low-LET Radiobiology

Low-LET radiation mainly acts indirectly by producing hydroxyl radicals accounting for $2/3^{rd}$ of its DNA damage compared to only $1/3^{rd}$ of direct action [40, 41]. Thus, under hypoxic conditions which often occur in tumors, may be resistant to this type of radiation and may reduce the death of cancer cells [4].

Another fall back arises from the cells radiosensitivity to radiation. Radiosensitivity is governed by the amount of DNA damage following treatment, as well as, the individual capacity to correctly repair the damage [42]. The cells susceptibility to proton-induced DNA damage has been found to be dependent upon the phase of the cell cycle in which the cells are in. This was observed when mammalian cells displayed differential responses to low-LET radiation. These cells portrayed high radiosensitivity shortly before and during mitosis but demonstrated radiation-resistance during DNA synthesis with maximum resistance occurring towards the end of the S-phase [43, 44]. These results demonstrated that proton-induced DNA damage was cell cycle specific to the reproductive M-phase and G1 of interphase, while resistant to S-phase cells [45].

These aspects are of a particular concern, as tumor cells which are low cycling or quiescent, are often localized in oxygen deprived tissues and are considered the most resistant to

proton radiation. These tumor cells have a larger capacity to recover from the low-LET-induced DNA damage, as their metabolic activity may be more readily equipped in dealing with the low-LET-induced radicals, thus allowing for their continued proliferation and failure to effectively kill the tumor.

1.6.2 Low-LET Proton Radiation and Particle Radiotherapy

Protons are clinically considered to be low-LET particles. Proton therapy is a type of particle therapy, distinguish from x-ray or gamma ray treatments that utilize massless photons, in which a proton is 1,836 times heavier than an electron. When compared to photons, proton beams are known to provide a superior dose distribution [30].

Particle radiotherapy utilizes ionizing radiation (forms electrically charged particles known as ions) which gradually deposits an increasing amount of energy in the cells of tissues along its path as it passes through [9, 33]. The dose of ionizing radiation given to the patients varies due to the sensitivity of the surrounding normal tissue around the location of the tumor, to minimize unwanted damage to normal tissue while still maximizing the damage to the cancer cells [4].

The depth at which majority of the particle beam's energy is deposited along the beam path at the end of its range is known as the "Bragg peak," named after Nobel prize-winning British physicist William H. Bragg. In charged particle radiotherapy, involving the carbon-ion and proton beams, this Bragg peak can be manipulated to incorporate the entire tumor to deliver the maximum dose of radiation to all the malignant cells, in a technique known as the spread-out Bragg peak (SOBP). Beyond the Bragg peak, there is a rapid falloff of the dose. The narrow region of the Bragg peak where a significant amount of energy from a particle beam is deposited

into the tissue, is the point at which LET is at its highest value [33]. Furthermore, the biological effectiveness of radiation modalities, i.e. ability to kill the cell, depends on the LET, total dose, fractionation rate and radio-sensitivity of the targeted cells or tissues [9].

1.6.3 Low-LET Proton Radiotherapy Facilities

There are around 62 proton therapy facilities currently in operation worldwide with more under construction and more than 131,000 patients have been treated since 2015 [20]. In the USA, only low-LET proton facilities are currently in operation but with the increasing interest in carbon-ion radiotherapy the future may hold a change from proton beam to construction of more carbon-ion beam facilities [46]. However, the current infrastructure required to generate and maintain a clinical proton beam is both bulky and expensive. Although these facilities are still less expensive than the infrastructure required for generating high-LET heavy ions, like carbon-ion beams, which is the likely reason for their majority of radiotherapy facilities worldwide as of today. The emergence of more effective treatments by use of high-LET carbon ion therapies, however, may lead to a shift from the construction of proton to carbon-ion radiotherapy facilities in the future.

1.6.4 General Concept of Proton Beam Production and Transport

Hydrogen gas is typically used to generate protons, as each hydrogen atom consists of a single proton and an electron. The negatively charged electrons and positively charged protons are separated via microwave energy which ionizes the hydrogen atoms, along with introducing a charge differential. Once separated the protons are initially accelerated using a linear accelerator before entering the cyclotron or synchrotron which accelerates the protons to more than half the

speed of light, which gives them a very high energy [47]. Moreover, the decision between using a cyclotron vs a synchrotron may depend on the intended use for the proton beam. Cyclotrons are more compact and have higher beam intensity, whereas synchrotrons can accelerate batches (pulses) of protons to the desired energy as well as each cycle can produce protons of different energy. Generally, the advantage of synchrotrons is that they have greater energy flexibility, smaller energy spread, and lower power consumption [48].

The cyclotron possesses two giant magnetized poles called dees. Rapidly alternating voltage is applied to the dees, which alternatively attracts and repulses the protons and creates a potential difference across the small gap between the dees and accelerates the protons as they zip across the gap. The magnetic field of the dees directs the path of the protons in a spiral pattern, resulting in protons towards the outer edge of the cyclotron to more faster and further. Using this principle, protons can be extracted at the desired predetermined energy into the beamline.

As the accelerated protons travel in the long beamline they are maintained under a vacuum to prevent proton–air interactions to prevent their degradation. Four magnets called quadrapoles create a magnetic field which keeps the stream of protons perfectly centered in the beamline and are utilized throughout this process to focus and bend the proton stream along the desired path and direct them towards the treatment rooms [47].

1.7 Cancers Effectively Treated by High-LET Carbon-Ion Radiotherapy

As location and radioresistance of certain tumors has created implications in their treatment, high-LET 290 MeV/n carbon-ions have shown promising results in effectively treating these tumors in which the other radiotherapy modalities have fallen short. Most notably these include; skull base tumors, lung cancer, head and neck cancer, prostate cancer, liver cancer,

pancreatic cancer, uterine cervical cancer, pelvic recurrences of rectal cancer, bone and soft tissue sarcoma. Furthermore, the treatment dose and the number of fractions of 290 MeV/n carbon-ion radiation varies as the size and location of these tumors may vary [46] (Table.1).

Carbon-ion radiotherapy was first applied for the treatment of patients with unrespectable locally advanced head and neck tumors that were very difficult to remove with surgery and hazardous to treat with chemotherapy. These tumors have been shown to be very effectively treated with carbon-ion beams, given a local control rate of around 80% [49]. 290 MeV/n carbon-ion beams have also demonstrated to be an effective treatment modality for melanomas, which are considered to be relatively radioresistant tumors [50, 51].

Table 1. Example of dosages and number of fractions used to treat cancers with carbon-ion radiotherapy.

Cancer Type	Dosage (GyE)	# of Fractions
Pancreatic Cancer	55.2	12
Glioblastoma (GBM)	24.8	25
Cervical Cancer	72	20
High Risk Prostate Cancer	51.6	12
Osteosarcomas & Soft Tissue Sarcomas (STS)	52.8-73.6	16
Hepatocellular carcinoma, Inoperable	60	12
Lung Cancer, Inoperable, Stage 1	60	4

Information available online at www.clinicaltrials.gov and www.umin.ac.jp/ctr.

Furthermore, 290 MeV/n carbon-ions have also been proven to be effective in treating pancreatic cancer, which is rarely curable due to its location, and is the 5th leading cause of death world-wide [46]. Surgery alone only provides a 5-year survival rate at less than 20% for pancreatic cancer patients, however when utilizing the combination of chemotherapy with carbon-ion irradiation, there has been a notable improvement in the 2-year overall survival rate. Bone and soft tissue sarcomas are also generally considered to be radioresistant to low-LET proton radiotherapy and are often inoperable. Carbon-ion radiotherapy offers the advantage in overcoming this radioresistance as well as in its local dose distribution precision, making it the prime candidate for treating chordomas and osteosarcomas as well [49].

1.7.1 High-LET Carbon-Ion Radiotherapy

Heavy ions (C, Ne, He) account for high-LET radiations. Usually accelerated atomic nuclei with an atomic number greater than 2 are classified as high-LET beams, because different biological effects are more clearly observed for these beams. For charged particles, protons and carbon-ions, their acceleration energy determines the depth of penetration of the particles into the body [52]. Moreover, as they travel deeper into the body, more energy is deposited and increases towards the end of their range to a high peak, resulting in a steep rise in the absorbed dose known as the Bragg peak [53]. Following the Bragg peak there is a steep drop of dose and in the case of carbon-ions, this dose falls to nearly zero [54].

When compared to photons, high-LET 290 MeV/n carbon-ion beams are more biologically effective if the same absorbed dose is applied, quantitatively expressed by having a higher RBE [20]. Carbon-ions are also heavier than protons, thus providing them with a larger RBE than protons as well. Furthermore, ions heavier than protons will have a reduced lateral

scattering, reduced range straggling, and an increased ratio of dose in the target relative to the entrance region, giving them superior physical dose distribution as well [45]. Moreover, a prior study revealed that increasing carbon-ions fraction dose resulted in a lower RBE for both tumor and normal tissues but did not decrease the RBE for the tumor as rapidly as it did for the normal tissues RBE. This demonstrated that the therapeutic ratio could increase rather than decrease even though the fraction dose was increased [30]. However, the disadvantage of carbon-ion beams used for radiotherapy comes from the nuclear fragmentation of the carbon-ion along its beam path, which does not happen with the use of proton beams. This results in nucleons at nearly the same velocity and direction capable of traveling longer ranges causing a fragmentation tail following the Bragg peak [55].

Carbon-ions were chosen for radiotherapy because of their biologically expressed dose distribution being far superior to the other ions, as well as, the high-LET components that insure controlling photon-resistant tumors [25]. Furthermore, their definite range and a sharp high-dose Bragg peak enables them to concentrate dose within a tumor, while minimizing dose to the surrounding normal tissue [56]. 290 MeV/n carbon-ions also travel in almost a straight line, so that a sharp and accurate collimation is possible, limiting the lateral scattering to only about 1.5 mm at a 20 cm depth in water, as compared to the lateral scattering of the low-LET proton beam of 6.5 mm [54]. This provides carbon-ion radiotherapy with a better dose distribution than with the proton beam. In addition, they also have a lower oxygen enhancement ratio, which is a desirable feature for eradication of radioresistant hypoxic tumors [57].

As radiotherapy aims to effectively kill tumor cells while minimizing dose to normal tissues to prevent toxicity [58], the fore mentioned factors contribute to carbon-ion as the superior radiotherapy modality, specifically for tumors previously displaying radioresistance.

1.7.2 High-LET Carbon-Ion Radiobiology

High-LET 290 MeV/n carbon-ion radiation mainly achieves DNA damage through direct action and is not cell cycle specific, as with low-LET radiations [59]. These beams also have a low oxygen enhancement ratio, meaning less indirect effects, and therefore they are better for treating hypoxic tumor cells that may be radioresistant to the low-LET therapies. Carbon-ion radiation is also associated with less DNA repair, more sophisticated repair mechanisms, as well as, carbon-ion treated cells portraying a very low repopulation rate. Furthermore, carbon-ion radiations tend to induce more small DNA fragments than low-LET radiation, which may explain why they have a larger RBE, since DNA double strand breaks are a major cause for radiation-induced cell death.

Although 290 MeV/n carbon-ion radiation is not considered to be cell cycle specific, cells that have undergone this treatment have portrayed considerably more pronounced cell cycle arrest, particularly in the G2-phase. This may be due to the carbon-ion radiation-induced occurrence of clustered DNA damage. DNA damage with multiple lesions is known as being "clustered" and defined as two or more closely associated DNA lesions that involve both strands. As a result, the cell requires more sophisticated demands for DNA repair [60, 61].

Furthermore, when carbon-ion irradiated cells are synchronized, there is a reduction of cell cycle-related radiosensitivity. This provides carbon-ion radiation with an additional advantage over conventional proton radiation, as cells in S-phase that are typically radioresistant to proton therapy are more sensitive to carbon-ion radiation, which may be a result from dysfunctional repair pathways [62].

1.7.3 High-LET Carbon-Ion Radiotherapy Facilities

The long-standing debate as to effectiveness vs cost of 290 MeV/n carbon-ion beam vs proton beam radiotherapies has hindered the spread of constructing the more expensive carbon-ion beam facilities worldwide. Even though carbon-ion beams have the clear advantage of treating tumors that are radioresistant against low-LET treatment modalities, as well as having a greater RBE [62].

There are several active proton therapy centers but only a few facilities which utilize carbon-ions are active throughout the world. This is due to the high initial capital cost in constructing these heavy ion therapy facilities at an estimated $300 million USD [57]. However, research portraying the emerging advantages of using 290 MeV/n carbon-ions as the superior modality in radiotherapy and their effectiveness in treating certain cancers, has led to an increase of these facilities worldwide, with more than 8 operational facilities and over 15,000 patients treated to date [56].

Japan has paved the way for the emergence of carbon-ion facilities, with 5 currently in operation as of 2015 and plans for construction of 3 more. Internationally there has also been a growing number of carbon-ion facilities. Countries such as Germany, Italy, China and Austria also have facilities currently in operation and South Korea, Taiwan and the USA are in varies states of development in construction [63].

1.7.4 HIMAC/NIRS

The National Institute of Radiological Sciences (NIRS) in Chiba, Japan, built the world's first medically dedicated heavy ion accelerator, called the Heavy Ion Medical Accelerator in Chiba (HIMAC). They started clinical application of 290 MeV/n carbon-ions in 1994 [56] and

since then more than 9,000 patients of been treated at this facility to date. Currently they have reached a treatment capacity of between 900-1000 patients per year [63, 64].

290 MeV/n carbon-ion radiotherapy at NIRS is typically given 4 times per week for 3 weeks with a total average of 13 fractions, however these may vary accordingly with tumor size and location [30]. Despite the current cost for patients for a carbon-ion radiotherapy treatment course (3.2 million yen/~28,000 USD), the clinical effectiveness demonstrated at their facility has led a continuous increase in the number of patients from both within and outside of Japan [63].

1.7.5 General Concept of Carbon-Ion Beam Production and Transport at HIMAC

Carbon-ion beam production and transport utilizes many of the same concepts as with proton beam production and transport. However, carbon-ions are generally accelerated at energies between 140-400 MeV in clinical settings, in contrast to energies between 65-200 MeV used when accelerating protons [25, 33].

HIMAC consists of an injector linear accelerator cascade, dual synchrotron rings with independent vertical and horizontal beam lines and three treatment rooms equipped with passive beam delivery systems. The carbon-ion beam is produced by injection of the 10 GHz-ECR ion into the linear accelerator cascade and is accelerated up to 6 MeV/n. Next, the carbon beam is fully stripped with a carbon-foil stripper and injected into the synchrotron rings where it is slowly extracted once it has accelerated to its desired energy. Lastly, the extracted carbon beam is delivered to its destination by the beam delivery system much like as in proton transport [49] (Fig.4).

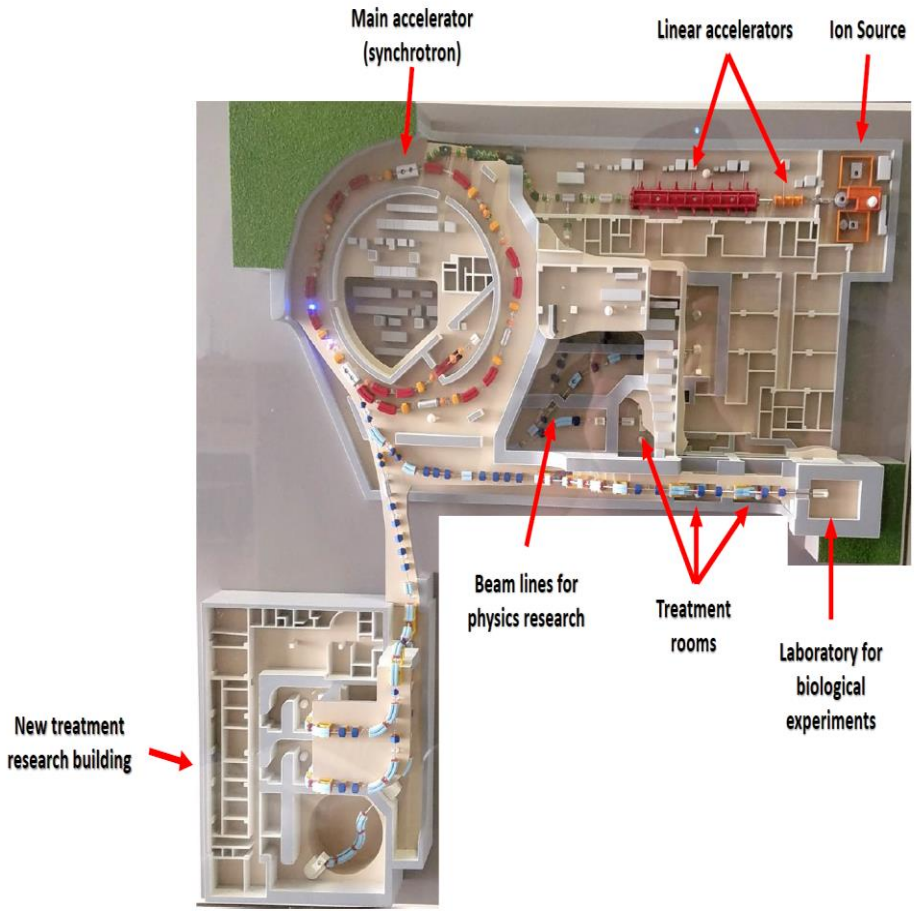

Figure 4. The HIMAC (Heavy-Ion Medical Accelerator in Chiba) facility. Photo image taken of a model HIMAC facility located at NIRS in Chiba, Japan.

1.7.6 Passive Carbon-Ion Beam Delivery at HIMAC

Due to the carbon-ion beam's Bragg peak being sharp and narrow, as well as only a few millimeters thick, to cover the various sizes of tumors with these beams, a passive beam delivery system utilizing a fixed spread out Bragg peak (SOBP) has been employed at HIMAC. The passive beam delivery system results in broader energy distributions due to the scattering in the beam path [65].

Once this narrow carbon beam in the delivery system from the accelerator reaches its destination, a pair of dipole magnets wobble this beam. The pencil beam, which controls the amplitudes of the magnetic fields, moves on a circular orbit around the original beam axis while the scatterer, thin metal foil, broadens the beam. By controlling the amplitudes of wobbling with the thickness of the scatterer, a uniform dose distribution is obtained at the isocenter.

Furthermore, to match the SOBP with the tumor size, a bar-ridge filter is utilized. The ridge filter was designed to produce a physical dose gradient of the SOBP so that the biological effect along the SOBP can be uniform. Next, a bolus compensator precisely matches the SOBP with a distal target shape. Finally, a multi-leaf collimator (MLC) and a patient collimator match the lateral dose distribution precisely with a lateral target shape [54] (Fig.5).

.

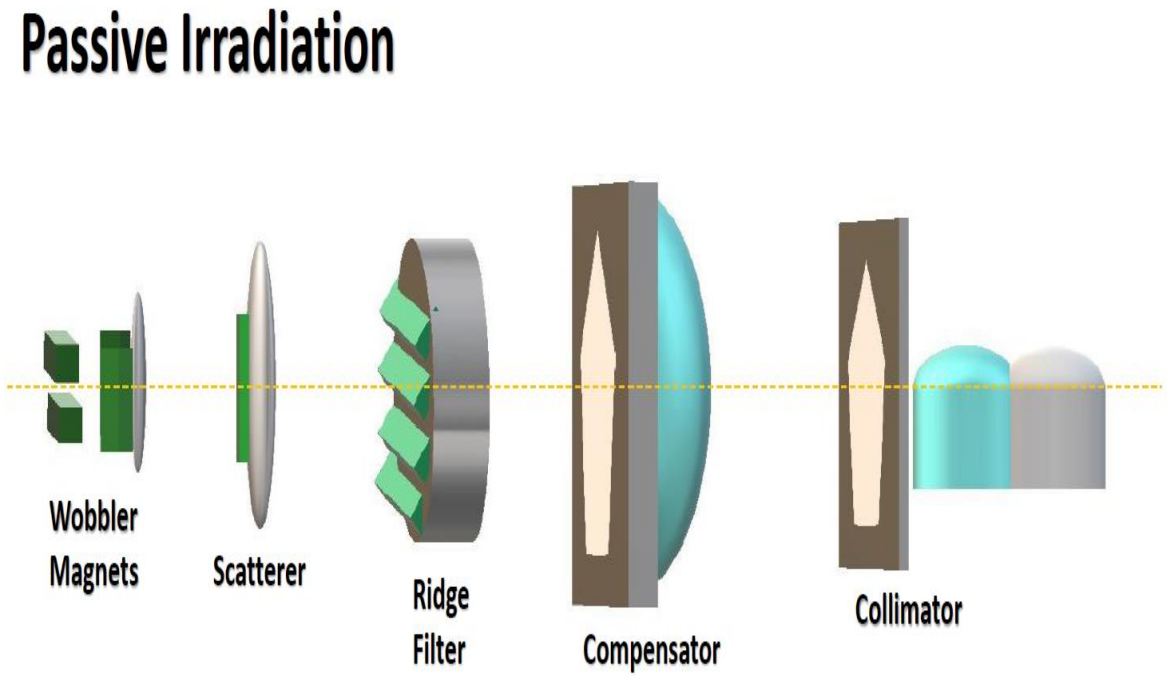

Figure 5. Passive beam delivery system utilized at HIMAC facility. Passive beam delivery system results in broader energy distributions due to the scattering in the beam path and allows utilization of spread out Bragg peak (SOBP) technique. Carbon-ion beam represented as yellow dashed line.

1.8 Specific Aims

It has been widely accepted that carbon-ion beams distribute their energy to the target tumor cells more precisely, however, there is still a lack of research regarding the degree in which the lethal dose is distributed amongst the normal cells adjacent to the target tumor cells. Clarifying this will help specify carbon-ion beam's precision of lethal dose distribution and aid physicians in accurately targeting tumor cells while sparing the normal healthy cells when applied in a clinical setting. Therefore, we hypothesized that the physical dose distribution of carbon-ion beams will differ than that of their biologically observed lethal dose distribution.

This study aims to clarify a more accurate biological representative assessment of the range in which monoenergetic 290 MeV/n carbon-ion beam irradiation induces cell death and cytotoxicity. Our development of a new survival fraction method in the cell survival assay, enabled us to analyze the precise and continuous cell killing effect of the monoenergetic 290 MeV/n carbon-ion beam with initial treatment doses of 1, 2, or 3 Gy, which has not been available thus far. Our previous studies have been carried out using several or many data points for specific depths, but fell short in defining this specific biological lethal dose range [3, 33].

We then further investigated how monoenergetic 290 MeV/n carbon-ion beam-induced cytotoxicity correlated with this biological lethal dose range utilizing the cytokinesis-block micronucleus assay (CBMN) utilizing. The cytotoxic effects were analyzed by quantitating the number of micronuclei in binucleated cells at different depths in our flasks with an initial treatment dose of 1 Gy, as micronuclei are a sign of a cytotoxic event and binucleated cells insured that these cells are going through cell division, as required for micronuclei formation [24, 66].

1.8.1 CHO Cell Line

We utilized the Chinese Hamster Ovary (CHO) cell line for our experiments due to their relatively small colony sizes, making them ideal to evaluate at only one specific depth in our flasks. Furthermore, there are many intrinsic factors that contribute to the cells tolerance of radiation. The genetic background of a cell is of importance, especially regarding the status of the DNA damage checkpoints, signaling pathways, and proficiency/capacity of the repair systems. Furthermore, radiation-induced cell death is also influenced by the rate of cell proliferation, cell cycle stage distribution, radical scavenger and anti-oxidative enzymes concentrations, and the metabolic status of the cells [20]. When addressing radiation-induced cellular damages it is of importance to select well established cell lines shown effective in radiation treatment in order to avoid background abnormalities.

CHO cells are a derived cell line from cells of the ovaries of Chinese hamsters. Chinese hamsters were first used in place of mice in 1919 for typing pneumococci. Then in 1957, Dr. Theodore T. Puck of the Dept. of Medicine at the University of Colorado, successfully isolated and established CHO cells in culture plates. He discovered that these cells were very resilient and their relatively fast generation times made them a great candidate for *in-vitro* cultivation. CHO cells soon became important for studying chromosomal abnormalities, due to having karyotype heterogeneity amongst their cell populations thus allowing for a low rate of spontaneous transformation, which has also made them ideal for quantitating radiation-induced micronuclei [67]. Furthermore, CHO cells low chromosome number (2n=22), quick doubling time (~14-17hrs) and relatively small colony size has also made CHO cells very useful models in radiation cytogenetics and tissue culture studies [68].

1.8.2 General Cell Survival Assay

Stopping tumor cell growth is the main goal behind radiotherapy, therefore the endpoint of cell survival is commonly used for *in-vitro* experiments. The most important measures of cell survival are its cellular viability, which is the ability of a cell to preserve its physical and metabolic integrity, and its clonogenicity, which is the ability of a cell to undergo cell division [20]. For a tumor to be eradicated, it is only necessary that cells be "killed" in the sense that they are rendered unable to divide and cause further growth and spread of the malignancy [69].

The *in-vitro* cell survival based assay, known as the clonogenic assay or colony formation assay, is based on the ability of a single cell to grow into a colony after treatment. A surviving cell that has retained its reproductive integrity and is able to proliferate indefinitely to produce a colony, defined as a group of at least 50 cells, is said to be clonogenic [69]. This assay has been the method of choice to determine cell reproductive death after treatment with ionizing radiation, as only a fraction of the seeded cells can produce colonies. It detects all cells that have retained the capacity for producing large numbers of progeny after treatments that can cause cell reproductive death resulting from damage to chromosomes, apoptosis, mitotic catastrophe, etc. [70] (Fig.6).

This technique was first described in 1956 by Puck and Marcus for implementing a cell culture technique for assessing culture dish plated single mammalian cells ability to form colonies. Their experiments portrayed the first radiation-dose survival curve for HeLa cells in culture irradiated with x-rays. Results from their experiments demonstrated that these mammalian cells were much more radiosensitive than previously assumed for cells in tissues and had a mean lethal dose range of 1-2 Gy, paving the way for this method to be implemented in future radiation experiments [70].

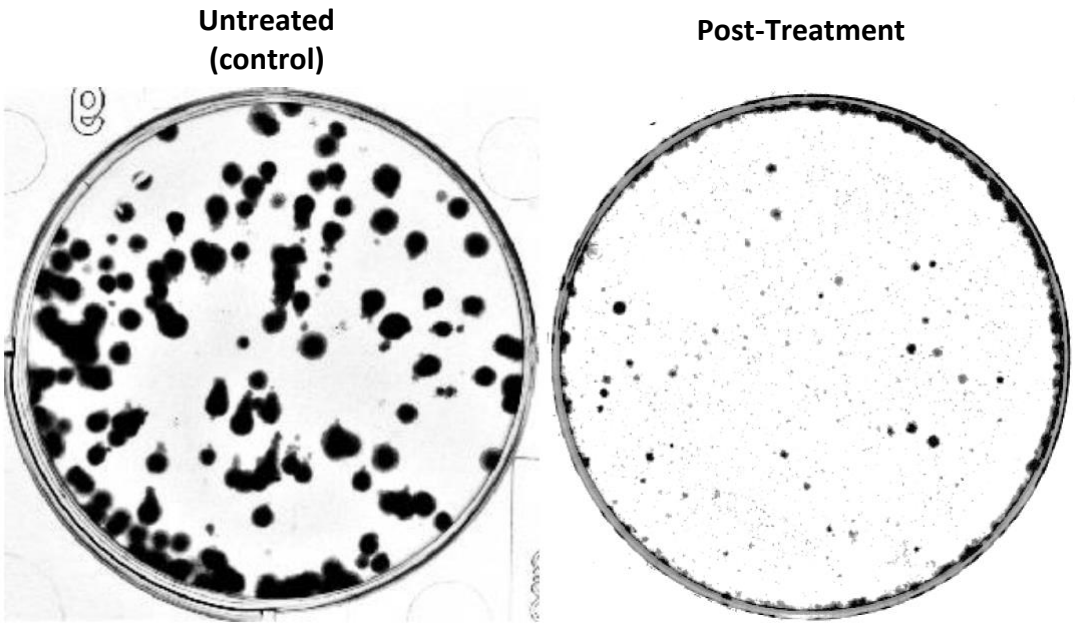

Figure 6. Example cell survival assay with UV-exposed CHO cultured petri dishes. (**Left**) Control portraying cell clonogenicity when untreated. (**Right**) All cells that have retained the capacity for producing large numbers of progeny after treatment.

In the clonogenic assay one must first address the plating efficiency (PE), as different cell lines vary in their PE's. The PE indicates the percentage of untreated cells seeded that grow into colonies [69]. CHO cells are known to possess a PE of 70-100% [70]. PE is the ratio of the number of colonies to the number of cells seeded:

When a parallel dish/flask is seeded with the same cells and undergoes treatment, the cells capable of forming colonies after 1-2 weeks of incubation prior to being fixed and stained, are said to have survived as they have retained their reproductive integrity. Evaluating the number of colonies allows for the survival fraction (SF) to be calculated [69]. Simply put, the SF is the number of colonies that arise after treatment of cells, expressed in terms of PE:

$$\boldsymbol{SF = \frac{\#\ of\ colonies}{\#\ of\ cells\ seeded\ \times \left(\frac{PE}{100}\right)}}$$

Using this information, a cell survival curve can be constructed. This depicts the relationship between the fraction of cells retaining their reproductive integrity and absorbed dose. Survival curves for mammalian cells are usually presented with dose plotted on a linear scale and surviving fraction on a logarithmic scale. In general, low-LET radiations, x-rays or gamma rays, produce a survival curve with an initial slope, followed by a bending region or shoulder, after which it tends to straighten again at higher doses which generally does not occur until doses exceeding those used as daily fractions in radiotherapy have been reached. Furthermore, high-LET radiations, heavy-ions, generally produce a straight line on a log-linear plot. In other words, high-LET radiation treatment survival approximates to an exponential function of dose [69] (Fig.7).

By quantifying cell survival at increasing depths in our flask with varying doses, allowed for us to determine the range at which each initial dosage could be considered lethal, as there

should be a dramatic decrease in survival fractions between these depths. Furthermore, we could address the carbon-ion beams observed biological Bragg peak, defined as the observed depth possessing the lowest number of colony formation. Moreover, this method enabled us to observe how this range increases with increasing initial dosages.

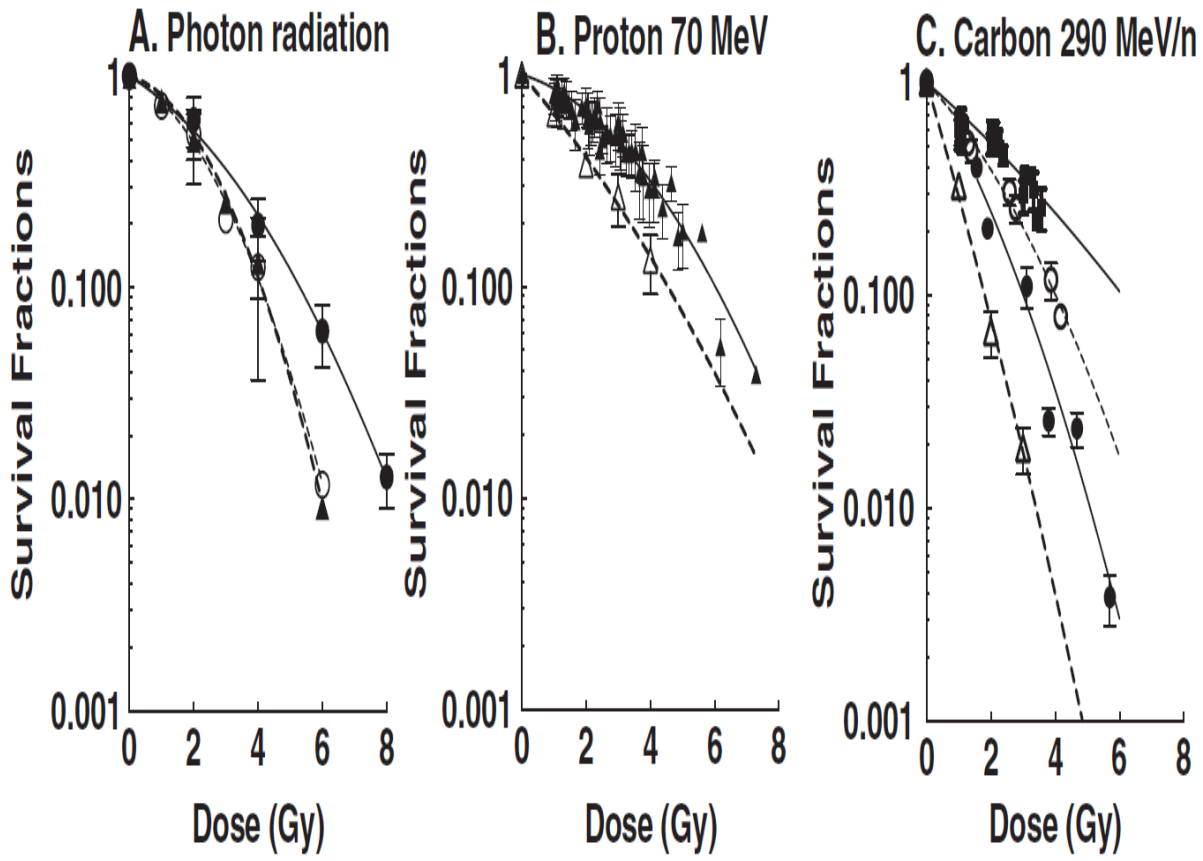

Figure 7. Example dose-response curves for different types of irradiation. A-B) Low-LET irradiations curve with an initial slope proceeding into a curved region and straightening out at higher dosages. **C)** Carbon-ion high-LET irradiation curve producing a straighter line. Figure taken from Fujisawa et al. [3]

1.8.3 Cytokinesis-Block Micronucleus (CBMN) Assay

It has been well established that the number of radiation-induced micronuclei (MN) is highly correlated with dose and quality of radiation. Moreover, dose-response curves for low-LET radiation have been observed to display a linear-quadratic dose-response, in contrast to high-LET radiation portraying a linear dependence dose-response [71]. Radiation-induced MN has been studied specifically for two reasons; for biological dosimetry when estimating the radiation dose, particularly after accidents, and as a predictor for tumor response in radiotherapy for the measurement of the intrinsic cellular radiosensitivity [66].

Chromosome breaks or whole chromosomes lagging during anaphase of mitosis leads to them being unincorporated into the daughter nuclei, thus resulting in the formation of small extranuclear bodies known as micronuclei (MN) [71]. These MN have a typical nuclear envelope which consists of two membranes, the lamina and nuclear pores [72]. MN are a sign of a genotoxic event or chromosomal instability, which would be difficult to quantitate via chromosomal aberration assay under conditions involving a large quantity of cells in a large flask. Furthermore, mitotic cell death/mitotic catastrophe is a major cause for solid tumor cell death [24]. The process is initially characterized by chromosome missegregation followed by aberrant mitosis or imperfect chromosome segregation, leading to the formation of multinucleated cells [20]. Quantitatively addressing the extent of micronuclei formation at increasing depths in our flask allowed us to decipher the range of which carbon-ion beams induce genotoxicity.

MN expression requires a cell to undergo a mitotic nuclear division and the procedure of choice for quantitatively evaluating micronuclei is via the cytokinesis-block micronucleus (CBMN) assay, developed by Fenech and Morley in 1985 [66, 71]. Other MN techniques prior to

the development of this assay were very imprecise due to cells undergoing only one cell division, which made it very difficult to precisely identify the MN within them separately from the total population of cells [73]. Furthermore, new chromosomal aberrations have also been observed in the second and third mitosis after irradiation, meaning that radiation-induced DNA damage is processed during the cell cycle and leads thereafter to the expression at later mitotic divisions [66]. For these reasons, the CBMN assay was developed allowing micronuclei to be evaluated in binucleated cells.

CBMN assay cells are incubated with the cytokinesis inhibitor, cytochalasin B, in a concentration that allowed for the inhibition of cytokinesis but still allowed Karyokinesis to be performed [66]. Furthermore, cytochalasin B itself was found not to produce micronuclei [73]. This allows for the formation of binucleated cells that can be easily detected under a microscope and MN expression occurs to the same degree as with normal cell division [74].

CHAPTER TWO

CARBON-ION RADIATION BIOLOGICAL LETHAL DOSE DISTRIBUTION

Introduction: Carbon-ions are known to display excellent dose-distribution and deposition around their Bragg peak, making them ideal for their use in radiotherapy. However, the precise range in which the carbon-ion beam distributes dosages that significantly induce cell death or genotoxicity surrounding its Bragg peak is not known.

Materials and Methods: Survival fraction or micronuclei formation of CHO cells cultured in T-175 flasks were compared at increasing depths in the flask following irradiation of 290 MeV/n monoenergetic carbon-ions with initial dosages of 1, 2, or 3 Gy for cell survival assays and 1 Gy for cytokinesis block micronuclei assays.

Results: Monoenergetic 290 MeV/n carbon-ions irradiation portrayed a biologically observed Bragg peak at the depth of 14.5 cm. Initial dosages of 1, 2, or 3 Gy irradiation portrayed significant reduction of survival fraction between the ranges of 14.0 – 14.5, 13.5 – 14.5 and 12.5 – 14.5 cm ($P < 0.0001$), as well as, reappearance of colony formation occurring at the depths of 14.72, 14.77 and 14.78 cm, respectively. Micronuclei formation coincided with our cell survival assays treated with 1 Gy initial dosage, as micronuclei frequency increased as the depth increased up to 14.5 cm, indicative of an increased genotoxicity up to this depth.

Conclusion: Monoenergetic 290 MeV/n carbon-ion beams portrayed a biological lethal dose range which increased with an increased initial dosage. Past the biologically observed Bragg peak there was also cell death, which may have been the result of nuclear fragmentation of the carbon-ion.

2.1 Introduction

Carbon-ion radiotherapy is a form of particle radiotherapy which utilizes ionizing radiation (forms electrically charged particles, ions) which gradually deposits an increasing amount of energy in the cells of tissues along its path as it passes through, known as linear energy transfer (LET) [9, 33]. The depth at which majority of the particle beam's energy is deposited along the beam path is known as the "Bragg peak," typically found at the end of the beams range. The Bragg peak region has the maximum energy deposition of high LET radiation. Beyond the Bragg peak, there is a rapid falloff of the dose [33]. Due to the carbon-ion Bragg peak regions having maximum biological effects from their high doses and high LET properties, it allows carbon-ions to achieve the fundamental principle of radiotherapy, to ensure precise localization of dose distribution to the target tumor while minimizing dose/damage to the surrounding normal tissues.

However, prior studies have revealed that nuclear fragmentations of the carbon-ions, known as the carbon-ion fragmentation tail, can continue travelling at nearly the same velocity and direction past the carbon-ion Bragg peak [55, 75]. Therefore, because of the carbon-ion sharp narrow Bragg peak and dose from the nuclear fragmentation, the extent of cell damage surrounding the Bragg peak remains enigmatic and must be addressed to further understand the precision of carbon-ion biological dose distribution and help define the extent of unwanted cellular damage surrounding the Bragg peak. These results will aid medical professionals utilizing carbon-ion beam radiotherapy to specify the dose distribution to the target tumor.

In this present study, we aim to fill a gap in current research involving the range in which the monoenergetic 290 MeV/n carbon-ion beam distributes biologically lethal dosages. Our

development of an *in-vitro* cell survival assay variant technique has enabled us with the ability to investigate biological effects near the Bragg peak precisely.

2.2 Materials and Methods

2.2.1 Radiation conditions

Carbon-ion ($^{12}C^{6+}$) beam irradiations were conducted at the National Institute of Radiological Sciences (NIRS) in Chiba, Japan. Carbon-ions were accelerated to 290 MeV/nucleon using the Heavy Ion Medical Accelerator in Chiba (HIMAC) synchrotron. Dose rates for the survival assays for carbon-ions were set at: 1 Gy/min, 2 Gy/min, and 3 Gy/min. Dose rates for the CBMN assays for carbon-ions were set at 1 Gy/min. Monoenergetic 290 MeV/nucleon carbon-ions have a LET value of 13 keV/μm on entrance. Irradiations were carried out at room temperature.

2.2.2 Fricke gel dosimeter

Ferrous xylenol gel was made in a T-175 cell culture flask containing: 4% (wt) gelatin 300 Bloom from porcine skin (Sigma-Aldrich Type Ag 2500), 50 mM sulfuric acid, 1 mM ferrous ammonium sulfate hexahydrate (Aldrich), 0.1 mM xylenol orange (Oxford Laboratory, India), and 96% Milli-Q water. After gel solidified, Flask was irradiated with 20 Gy carbon-ion beam. Carbon-ion beam entered from bottom (non-capped end), as described in irradiation procedure and cell survival assays. 30 min following irradiation, flask was scanned to capture image.

2.2.3 Cell culture

Chinese hamster ovary (CHO) cells were kindly supplied by Dr. Joel Bedford (Colorado State University, Fort Collins, CO). Cells were grown and maintained in α-MEM (Invitrogen, Carlsbad, CA) supplemented with 10% heat inactivated fetal bovine serum (Sigma, St. Louis, MO) and 1% antibiotics and antimycotic (Invitrogen, Carlsbad, CA), maintained at 37°C in incubators at 5% CO_2 and 100% humidity. Doubling times were approximately 12hrs for this cell line.

2.2.4 Irradiation procedure for cell survival assays

Cultured cells were trypsinized and re-suspended into growth medium. Once re-suspended, 50 mL of media containing 30,000 CHO cells were placed into their appropriately labeled T-175 cell culture flask (Sigma, St. Louis, MO) approximately 1 hr prior to irradiation. All flasks were organized and irradiated independently with a dosage of either 1, 2 or 3 Gy. All flasks beam entry point was at the bottom of the flask (non-capped end) (Fig.8). Immediately following radiation, all cells were incubated for a period of 7 days for colony formation. After this culturing period, each culture flask was then washed with 0.9% NaCl, fixed in 100% ethanol and stained with 0.1% crystal violet. A minimum of three independent experiments were carried out for each dosage of radiation studied.

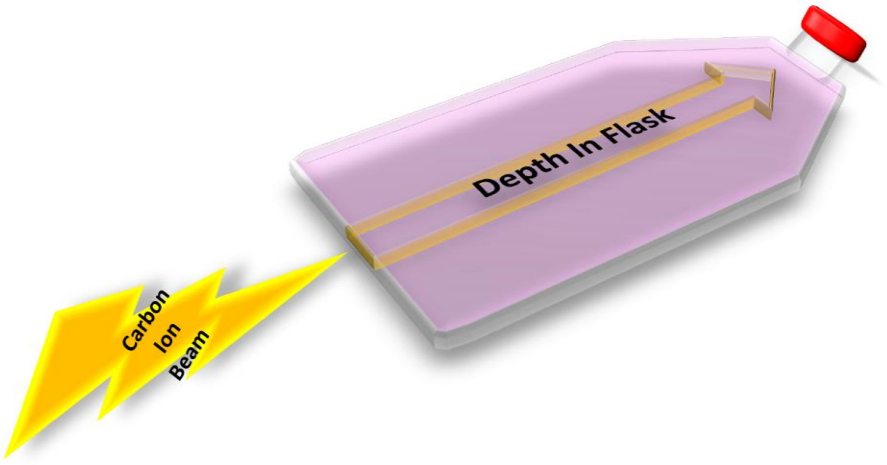

Figure 8. Illistration of carbon-ion beam entry. Prior to irradiation, cell culture flasks were placed upright with the capped end opposite to the beam source. Flasks were irradiated independently from each other and beam entry site, depected by lightnight bolt, was at the bottom of the flask (non-capped end).

2.2.5 Survival fraction calculation for cell survival assays

Survival fraction was obtained at depths of: 2.0, 4.0, 6.0, 8.0, 10.0, 10.5, 11.0, 11.5, 12.0, 12.5, 13.0, 13.5, 14.0, 14.5, 15.0, 15.5, 16.0, 16.5, 17.0, 17.5, and 18 cm from carbon-ion beam entry at the bottom of the flask (non-capped end). To quantitate the survival fraction at each of our evaluated depths, they were scored for every millimeter along the width of the flask either possessing a surviving colony, defined as a colony containing > 50 cells, or not possessing a surviving colony and the average value was calculated (Fig.9). This approach was repeated for a minimum of three independent experiments per each one of our initial dosages of 1, 2 or 3 Gy.

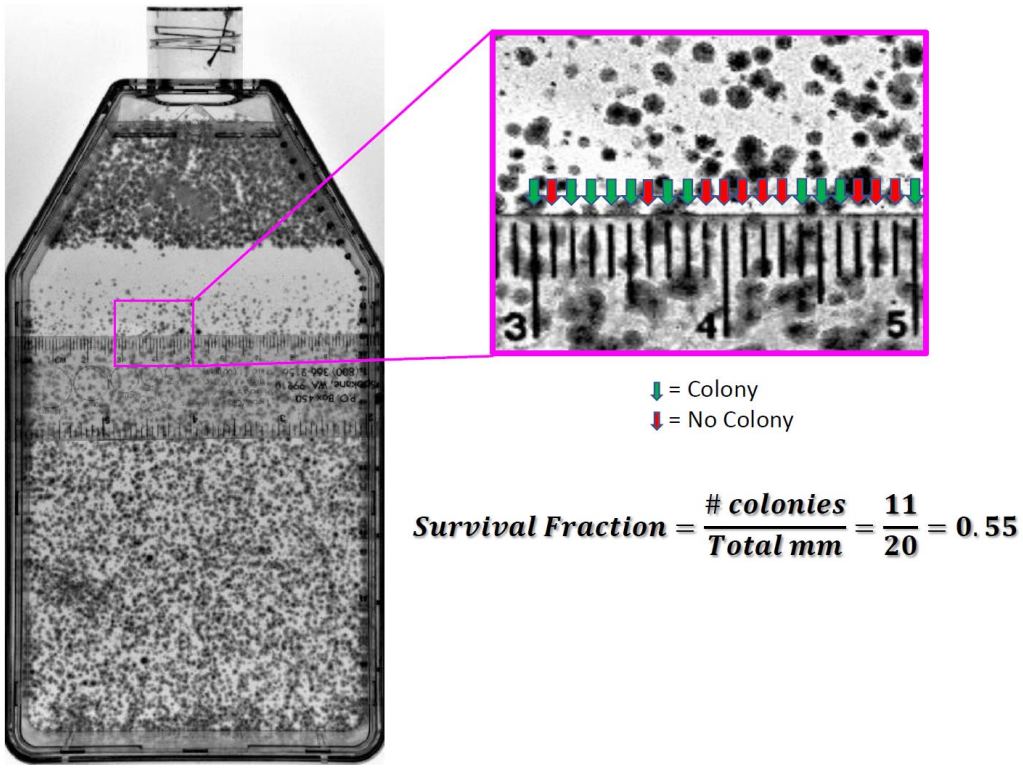

Figure 9. Example scoring procedure for calculating survival fraction. At each specified depth, surviving colony or no colony was addressed for every millimeter across the widths of the flask. Surviving colony was defined as a colony containing > 50 cells. Survival fraction was equal to the number of surviving colonies over the total width of flask (mm).

2.2.6 End of Bragg peak: reappearance of colony formation

Reappearance of colony formation depths were determined by measuring the distance from the bottom of the flask at beam entry to the first appearing cells of a colony following the biological Bragg peak. This was done at three locations for each flask and repeated for each of the three independent experiments per each one of our initial dosages. Average values were then extrapolated for each of our initial dosages.

2.2.7 Computer generated surface plots of colony formation

Survival assay flasks were imaged with the BIO-RAD ChemiDoc chemiluminescent imager (BIO-RAD, Hercules, CA) via ImageLab^{TM} 2.0.1 software (BIO-RAD, Hercules, CA) under white trans illumination utilizing a standard emission filter. These images were binarized and converted into a surface plot via MATLAB^{TM} software (MATHWORKS, Natick, MA). Pixel differences addressed colony distribution incorporating all colonies between the widths of 3 – 8 cm and depths of 2 – 17.5 cm.

2.2.8 Dose response curve

Dose response curve was generated utilizing the survival fraction values obtained from our cell survival assay experiments and the radiation physics quantitative values, including dose distribution and LET distribution for carbon-ion beams. The radiation physics quantitative values were kindly supplied by NIRS and were adjusted for our evaluated depths, with highest dosage values indicated in red and highest LET values indicated in pink (Tables.2-3).

Table 2. Radiation physics calculated quantitative values provided by NIRS

Depth (cm)	Dose (Gy)			LET (keV/μm)
0	1	2	3	13.4
6.483	1.048218	2.0964	3.1447	15.8
9.617	1.174004	2.348	3.522	18.8
11.61	1.400419	2.8008	4.2013	23.6
12.651	1.668763	3.3375	5.0063	29.5
13.212	1.937107	3.8742	5.8113	39.3
13.571	2.255765	4.5115	6.7673	47.2
13.802	2.683438	5.3669	8.0503	58.1
13.908	3.031446	6.0629	9.0943	67.7
14.022	3.773585	7.5472	11.321	91.5
14.085	4.515723	9.0314	13.547	137
14.139	4.817191	9.6344	14.452	230
14.202	2.880503	5.761	8.6415	337
14.253	0.9559748	1.9119	2.8679	273
14.316	0.3878407	0.7757	1.1635	42.4
14.84	0.3450734	0.6901	1.0352	29.4
14.729	0.3144654	0.6289	0.9434	27.6

Table 3. Adjusted dose values for our experimental depths.

Depth (cm)	Dose (Gy)		
0	1	2	3
6	1.045	2.061	3.091
8	1.107	2.215	3.323
10	1.215	2.43	3.644
10.5	1.27	2.539	3.809
11	1.327	2.654	3.981
11.5	1.387	2.774	4.161
12	1.495	2.991	4.486
12.5	1.627	3.253	4.88
13	1.831	3.705	5.492
13.5	2.179	4.353	6.712
14	3.497	7.541	11.311
14.5	0.36	0.719	1.079
15	0.31	0.619	0.928

2.2.9 Irradiation procedure and Cytokinesis-Block Micronucleus Assay (CBMN)

Cultured cells were trypsinized and re-suspended into growth medium. Once re-suspended, 50 mL of media containing 1,000,000 CHO cells were placed into T-175 cell culture flask approximately 1 hr prior to irradiation. Immediately following radiation, cells were treated with 250 μL of cytochalasin B (1mg/mL) for a final concentration of 5 μg/mL and incubated for a period of 1 day. After this incubation period, cells were fixed by: discarding the media, washing with PBS, followed by treatment of 20 mL 75 mM KCl for 10 sec and then discarded, followed by treatment with 20 mL solution of Acidic Acid and Methanol (1:1) for 10 sec and then discarded. After fixing, cells were stained for 5 min with a solution composed of 30 mL Gurr (Gibco®, Waltham, MA) with 1.5 mL Giemsa (Gibco®, Waltham, MA). A minimum of three independent CBMN assay experiments were carried out for our irradiated samples as well as our control. Micronuclei frequency was determined by the number of micronuclei divided by the number of binucleated cells. Approximately 150 binucleated cells in irradiated samples were evaluated at each depth of 2.0, 10.0, 12.5, 14.5, and 16.5 cm. Since our control samples were independent of depth, approximately 150 binucleated cells were evaluated regardless of depth. Example of binucleated cells evaluated that either expressed or not expressed micronuclei as depicted in Figure 10.

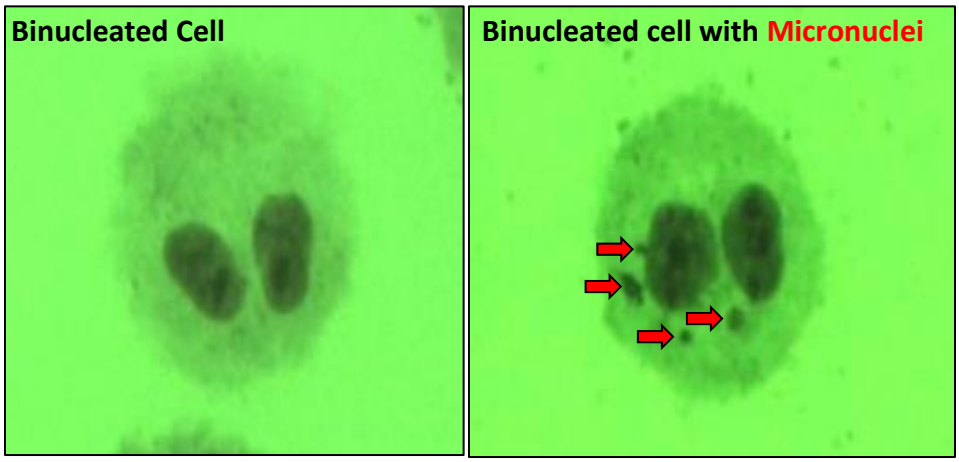

Figure 10. CBMN assay depiction of evaluated cells. CBMN assay cells are incubated with the cytokinesis inhibitor, cytochalasin B, to allow formation of binucleated cells to ensure that our evaluated cells underwent cellular division. (**Left**) Image of one of our binucleated cells not expressing micronuclei. (**Right**) Image of one of our binucleated cells expressing micronuclei. Red arrows represent evaluated micronuclei present in the cell.

2.2.10 Statistical analysis

All experimental data were analyzed via Prism 5^{TM} software (GraphPad, La Jolla, CA, USA). One-way analysis of variance (ANOVA) and Dunnett's multiple comparison test was conducted for statistical significance. P-values of < 0.05 were considered to indicate differences that were statistically significant.

2.3 Results

2.3.1 Fricke gel dosimetry

To address the depths displaying observable changes in dosage, we utilized Fricke gel dosimetry as a visual representation of the carbon-ion beam dose distribution in our T-175 flasks, as it has been reported as a quality method for detecting dose distribution [76, 77] (Fig.11). Irradiation oxidizes Fe^{2+} to Fe^{3+} which changes the color of the originally yellow gel to various orange-color combinations depending on the dosage at that specific depth. This allowed us to visually observe the dose distribution at various depths in our flask. Increasing dosages indicated via color change in our flask were as follows; orange-pink, indicating low dosage was observed from beam entry (non-capped end) to ~8.0 cm; orange-light red, indicating an increase in dose was observed between ~8.0 – ~12.5 cm; orange-purple, indicating a further increase in dosage was observed between ~12.5 - ~13.8 cm; orange-dark red, indicating the highest dose values was observed between ~13.8 -~14.5 cm. Beyond ~14.5 cm, the Fricke gel remained its originally yellow color, indicating a steep drop off of dosage shortly following this depth. These results indicated that our biologically observed Bragg peak should be within the ranges of depths of 13.8 - 14.5 cm (Fig.11).

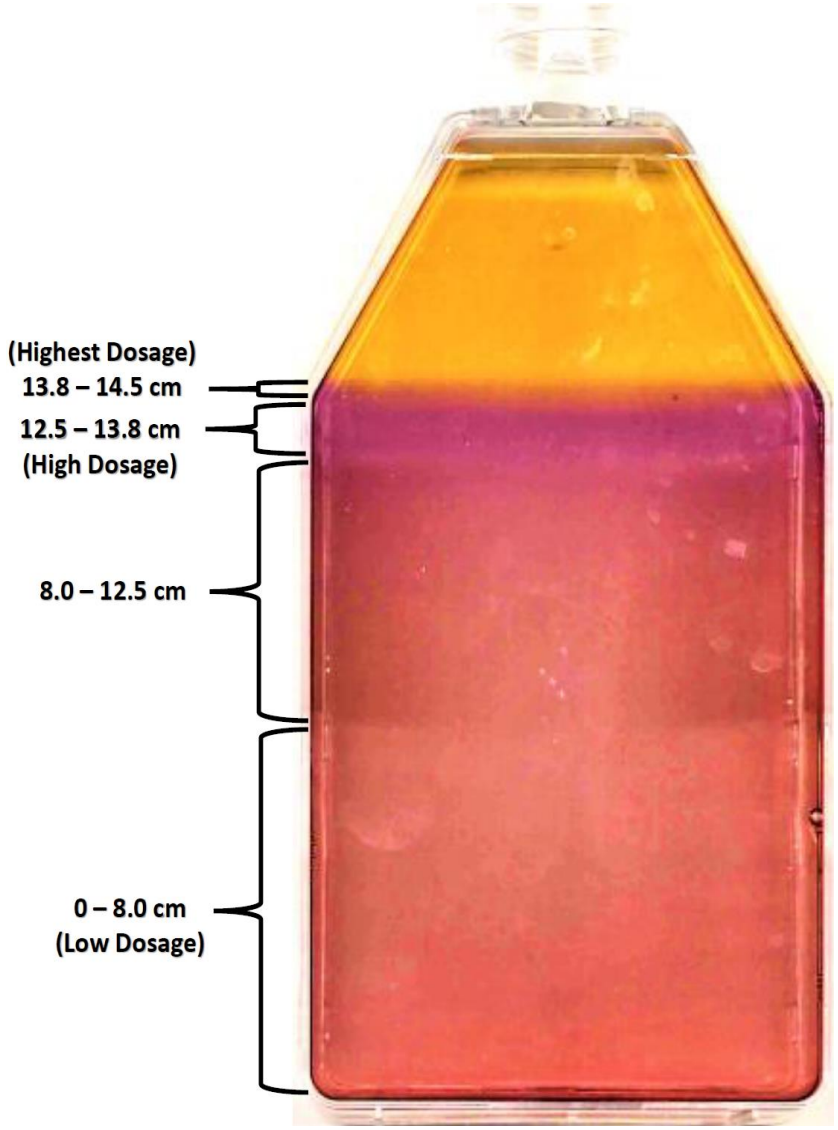

Figure 11. Fricke gel dosimetry visual representation of carbon-ion beam depth vs dose distribution in our T-175 cell culture flask. Fricke gel was irradiated with 290 MeV/n carbon-ion at an initial dosage of 20 Gy. Carbon-ion beam entered from bottom of flask (non-capped end). Color changes in Fricke gel are representative of dose at that depth. Fricke gel original color of yellow represents no observable dosage. Orange-pink, representative of very low observable dosages. Orange-light red, representative of low observable dosage. Orange-purple, representative of high dosages. Orange-dark red, representative of the highest dosage.

2.3.2 Visual representation of cell survival assays and biologically observed Bragg Peak

CHO cells cultured in T-175 cell culture flasks were irradiated with 290 MeV/n monoenergetic carbon-ion beams at either 1, 2, or 3 Gy initial dosage. Under all irradiation conditions, there was little to no observable colony formation at the depth of 14.5 cm. Therefore, this depth was regarded to as our biologically observed Bragg peak, as we suspected colony formation should be at its lowest when dose was at its highest value. Furthermore, there was a visually observable range prior to and following our biologically observed Bragg peak portraying apparent reduction in colony formation, which we referred to as the lethal dose range. This lethal dose range demonstrated to increase as the initial dosage increased. Following this range upstream from our biologically observed Bragg peak, there was a noticeable increase in colony formation, suggesting a dramatic decrease in dosage (Fig.12).

2.3.3 Proximal end of biological lethal dose range

All irradiation conditions displayed the general trend of a decrease in survival fractions as the depth in the flask increased up to the depth of 14.5 cm, in which there were the least number of surviving colonies. Furthermore, each increase in dose portrayed a greater decrease in survival fraction at each quantified depth up to 14.5 cm. At depths of 15 cm and beyond, the rapid increase in survival fraction was similar regardless of initial dose (Fig.13A).

Significant changes in survival fractions at each evaluated depth was addressed as compared to the survival fraction at the initial evaluated depth at 2.0 cm for each of our experimental initial radiation dosages. Flasks treated with 1 Gy initial irradiation portrayed significant decrease in survival fractions at depths of 14.0 cm and 14.5 cm ($P < 0.0001$) (Fig.13A). Treatment with 2 Gy initial irradiation portrayed significant decrease in survival

fractions at depths between 12.5 – 14.5 cm ($P < 0.05$) with the most significant decrease occurring between the depths of 13.5 – 14.5 cm ($P < 0.0001$) (Fig.13B). Treatment with 3 Gy initial irradiation portrayed a significant decrease in survival fractions between the depths of 12.0 – 14.5 cm ($P < 0.05$), with the most significant decrease being between 12.5 – 14.5 cm ($P < 0.0001$). Furthermore, 3 Gy initial dosage treatment portrayed the lowest survival fraction at the initial quantified depth of 2.0 cm (Fig.13D), resulting in significant increases in survival fractions for the depths between 15.5 – 18.0 cm ($P < 0.0001$) (Fig.13C).

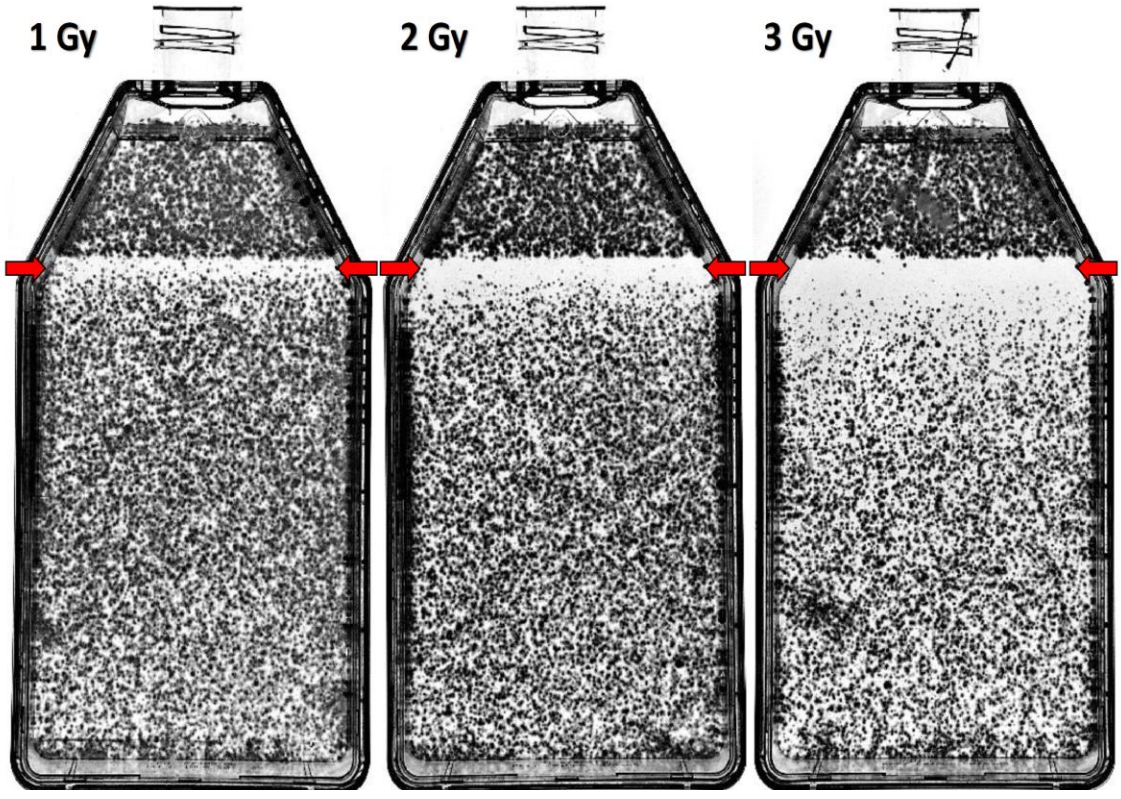

Figure 12. Images of cell survival assay T-175 cell culture flasks. Cell survival assays were conducted with T-175 cell culture flasks, irradiated with 290 MeV/n carbon-ions at either 1, 2, or 3 Gy initial dosage. The depth of 14.5 cm portrayed few to no observable colonies, thus referred to as our biologically observed Bragg peak. The range in which there was a clear decrease in colony formation surrounding this biologically observed Bragg peak was referred to as our lethal dosage range. This range was observed to increase as the initial dosage increased. Red arrow: indicates depth of 14.5 cm.

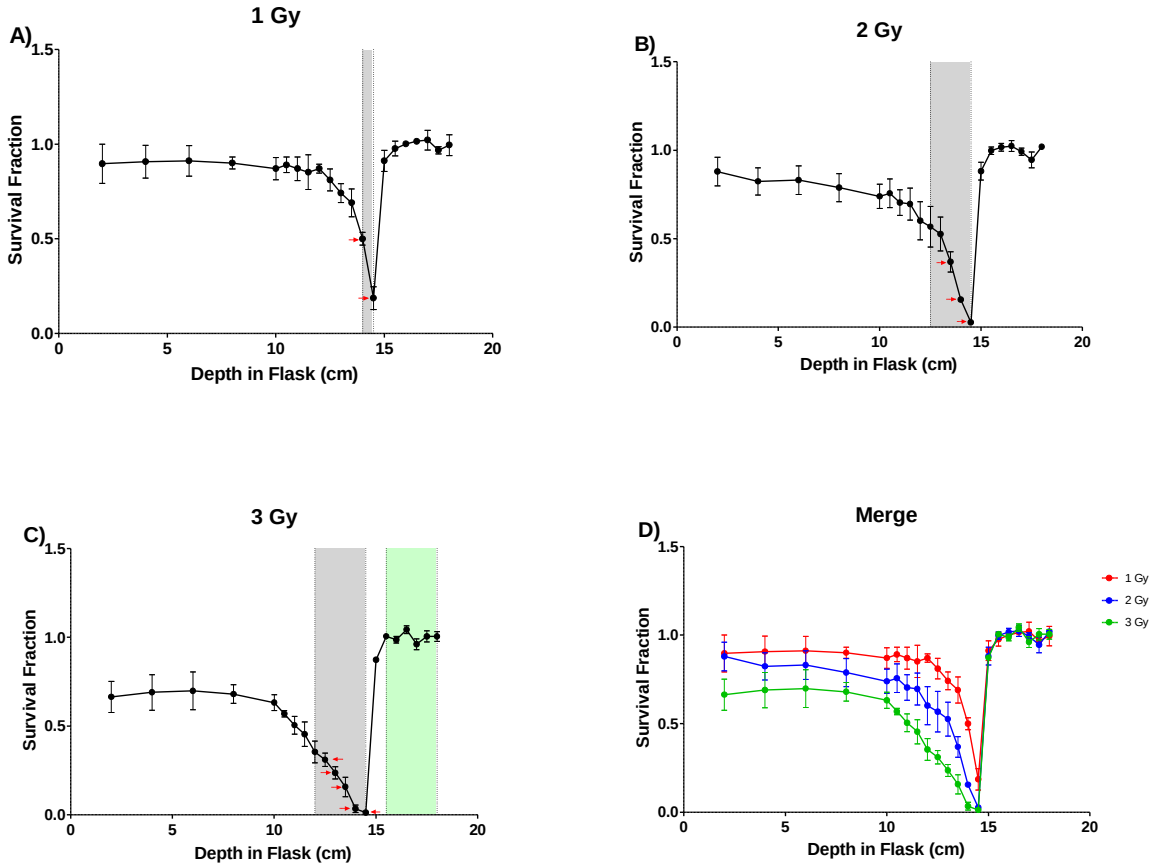

Figure 13. Cell survival curves at each depth in flask. Cell survival assays were conducted in T-175 cell culture flasks containing CHO cell line, irradiated with 290 MeV/n carbon-ions at initial dosages of 1, 2, or 3 Gy. Each experimental flask was irradiated independently from one another. **(A-C)** Significant changes in colony formation under each initial dosage was addressed by colony formation at each of our evaluated depths as compared to colony formation at the initial evaluated depth of 2.0 cm. Areas highlighted in gray are representative of a significant decrease in colony formation ($P < 0.05$), with red arrows representing depths with the most significant decrease ($P < 0.0001$). Areas highlighted in green are representative of a significant increase in colony formation ($P < 0.05$). **(D)** Merge of all cell survival curves demonstrating a clear decrease in colony formation as initial dosage increased up to 14.5 cm, with a rapid increase in colony formation at depths from 15.0 to 18.0 cm. Error bars indicate standard errors of the means from a minimum of three independent experiments per each one of our initial dosages.

2.3.4 Computer generated surface plot

To ensure that our chosen evaluation depths of our prior cell survival assays depicted accurate survival fractions, a surface plot was generated via MATLAB^{TM} software for each of our cell survival experimental initial dosages (Fig.14). This method allowed for the evaluation of colony formation at all depths but could not decipher between surviving colonies vs non-surviving colonies, i.e. if the colony contained > 50 cells. However, these results portrayed a clear range in which there was a clear decrease in colony formation, which increased as the initial dosage increased. Moreover, the depth possessing the least number of colonies was at 14.5 cm and following this depth there was a sharp increase in colony formation under all initial dosage conditions. Therefore, the consistencies between our surface plots and our prior survival assay results supported that our chosen evaluation depths were an accurate depiction of survival fraction changes.

2.3.5 Dose-response curve

Using data acquired from the NIRS depicting their depth vs calculated dosages and LET values combined with our observed cell survival results for evaluated depths between 6.0 – 15.0 cm, survival was portrayed by the given calculated dosages adjusted for our specific depths (Table.3, Fig.15). For LET values both < and > 50, survival fractions were shown as dependent on radiation dose, as they decreased as the dose increased. Intriguingly, survival fractions for each of our experimental initial radiation dosages of 1, 2 or 3 Gy adjacent to the calculated Bragg peak possessed a dramatic decrease even though the calculated dosage depicted a steep drop-off of dosage at these depths. Moreover, past the adjacent depth to the calculated Bragg peak, survival fraction dramatically increased as the dose further decreased.

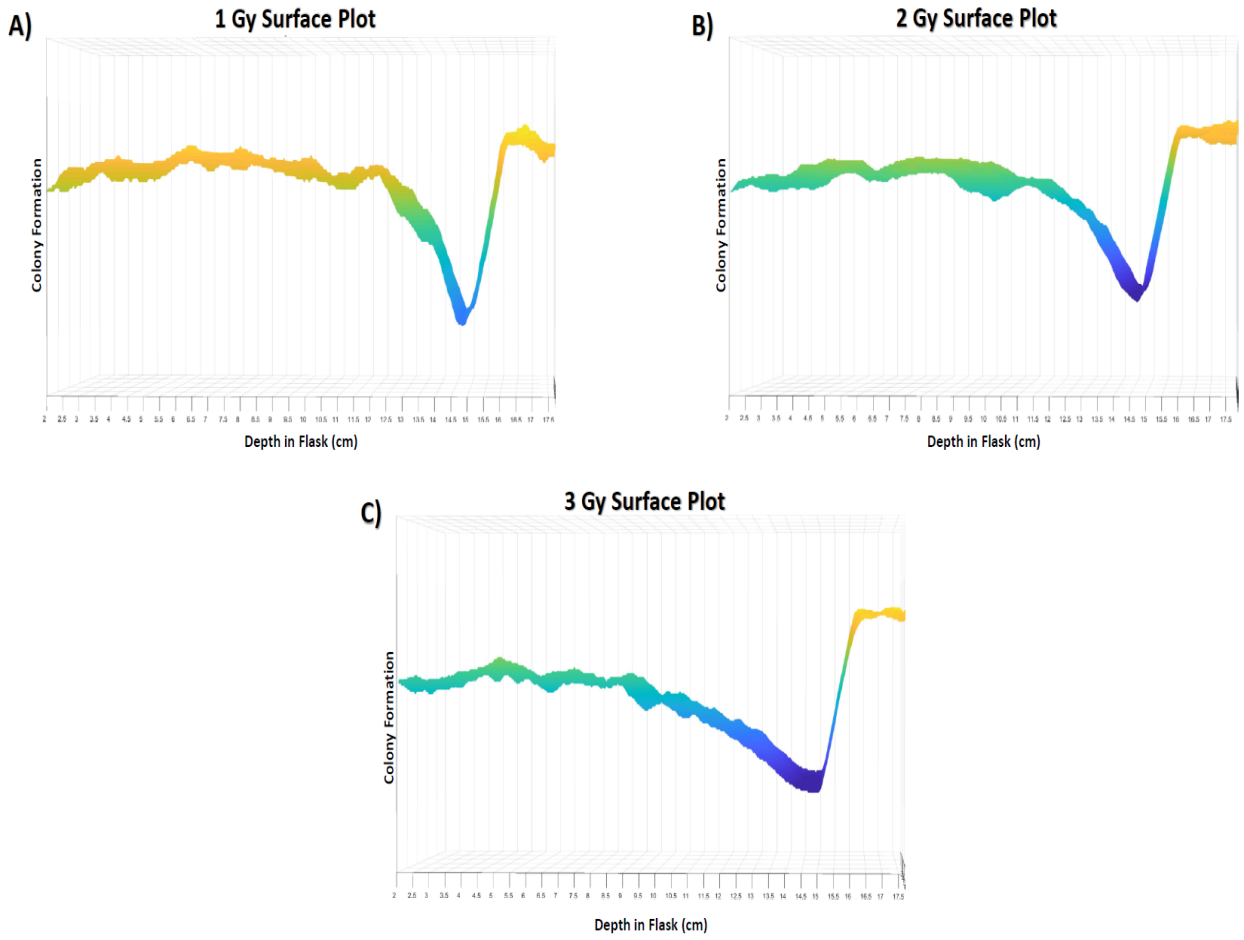

Figure 14. Surface plot representation of colony formation at increasing depths for each experimental initial carbon-ion dosage. Surface plot allowed for the evaluation of colony formation at all depths in flask but could not differentiate between surviving or non-surviving colonies, i.e. colonies containing >50 cells. The surface plot displays the relative density of cell colonies as a function of flask depth and flask width; higher densities yielded higher arbitrary values on the Z-axis and vice versa. As initial dosage increased survival fraction decreased up until 14.5 cm. Under all initial dosage treatments there was a clear decrease in colony formation around the depth of 14.5 cm preceded by a rapid increase in colony formation. These results were consistent with the prior survival assay technique. The color scheme used was standardized among all plots. The order of the color scheme from maximum cell colony density to minimum cell colony density (few or no cells present) is as follows: yellow, orange, green, blue, and purple, respectively.

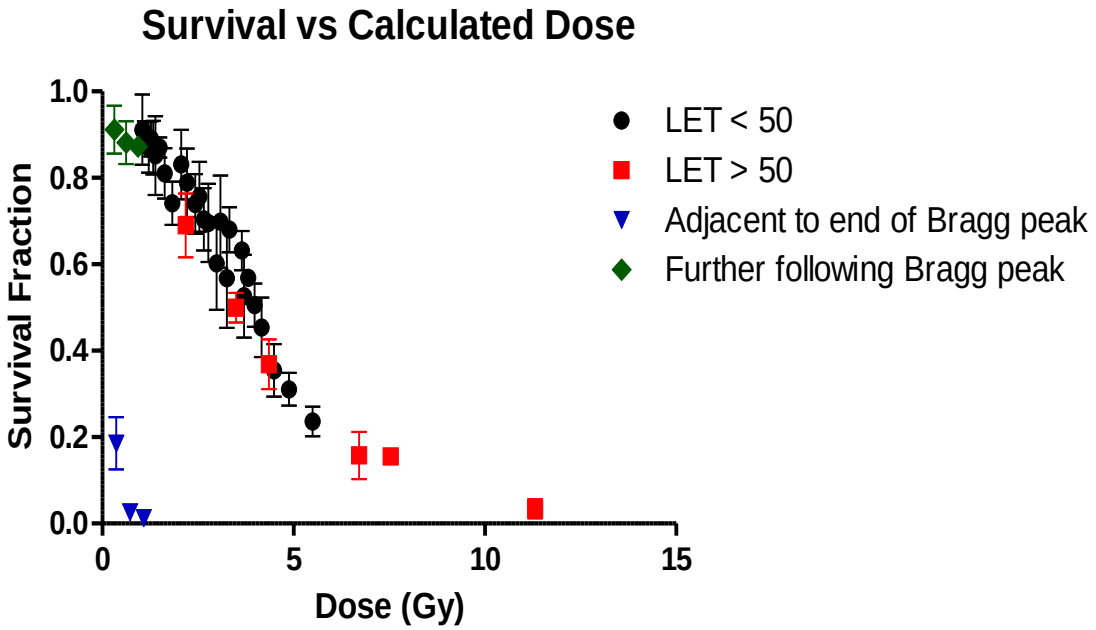

Figure 15. Dose response curve for carbon-ions. Survival fraction per dose was calculated from Figure 13 and Table 3. Circles represent LET < 50 keV/μm and red squares represent LET > 50 keV/μm (LET values obtained from Table 2). Blue triangles represent survival fractions adjacent to the end of the calculated Bragg peak (i.e. highest calculated dose) and green diamonds represent survival fractions at deeper depths than those adjacent to the end of the calculated Bragg peak. Error bars indicate standard errors of the means from as many as three independent experiments per our three initial dosages.

2.3.6 Distal end of biological lethal dose range

To determine the depth at which the dosage returned to a biologically non-lethal dose following our biologically observed Bragg peak at 14.5 cm, we quantitatively measured the depth at which there was colony reformation under each of our experimental initial dosages. This depth was representative as the end of our biologically observed lethal dose range. Reappearance of colonies were observed for initial dosages of 1 Gy, 2 Gy and 3 Gy at the depths in the flask of 147.22 ± 0.4 mm, 147.77 ± 0.4 mm and 147.89 ± 0.3 mm, respectively. These results indicated that as the initial dosage increased from 1 Gy to 3 Gy the depth of colony formation significantly increased as well ($P < 0.05$) (Fig. 16).

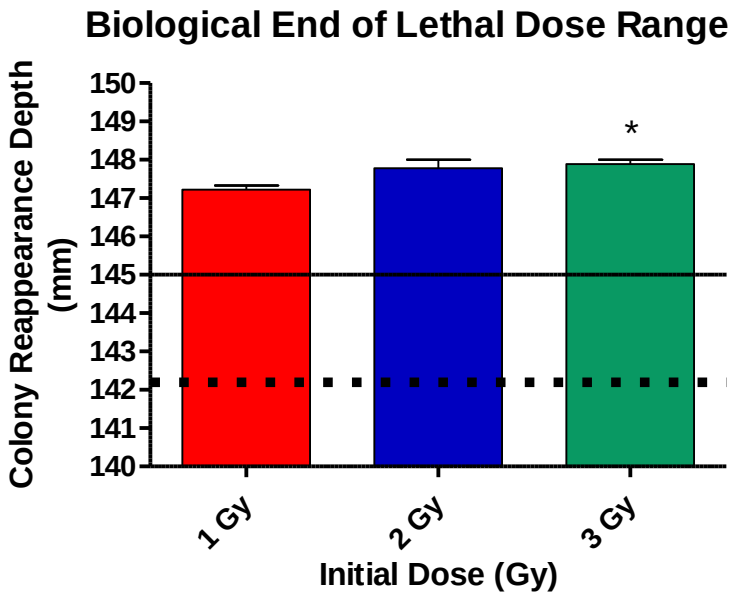

Figure 16. Depths of reappearance of colony formation following the biologically observed Bragg peak. Colony reformation under all initial dosage treatments between depths of 14.7 – 14.8 cm. Increase of initial dosage led to significant increase in depth of colony reappearance ($P = 0.0496$). Colony reappearance depth of 3 Gy was significantly increased as compared to 1 Gy ($P < 0.05$). Straight line representative of our biologically observed Bragg peak. Dotted line representative of NIRS calculated Bragg peak. Error bars indicate standard errors of the means from as many as three independent experiments per each initial dosage.

2.3.7 Micronuclei formation vs depth in the flask

Micronuclei (MN) were quantitatively evaluated to address carbon-ion beam irradiation-induced genotoxicity. CHO cell cultured T-175 flasks were subjected to an initial dose of 1 Gy carbon-ion beam irradiation entering from the bottom of the flask. The CBMN assay was utilized, as it has been shown to be the procedure of choice to quantitatively evaluate MN formation [66, 71]. The formation of micronuclei per ~150 binucleated cells was quantified at depths coinciding with observed changes in our 1 Gy initial dose irradiated cell survival results. We chose depths at; 2.0 cm and 10.0 cm, as there was a relatively small decline in colony formation between these depths. Depths at 12.5 cm and 14.5 cm, because the steepest decline in colony formation started between these depths and ended at 14.5 cm. Our final evaluated depth was at 16.5 cm, as this depth possessed the relatively highest number of colonies.

Micronuclei formation increased in correspondence with an increased depth in the flask up to the evaluated depth of 14.5 cm. Past this depth, at 16.5 cm, there was a significant decrease in micronuclei formation ($P < 0.05$), with mean values of micronuclei per binucleated cells of 2.865 ± 2.3 at 14.5 cm to 0.919 ± 0.30 at 16.5 cm. However, micronuclei formation at any of our evaluated depths was not significant as compared to our control ($P = 0.2088$). It is important to note that micronuclei formation at the depth of 16.5 cm fell between micronuclei formation at the depths of 2.0 cm and 10.0 cm, with mean values of micronuclei per cells of 0.837 ± 0.32 and 0.981 ± 0.28, respectively, and 0.919 ± 0.30 for 16.5 cm.

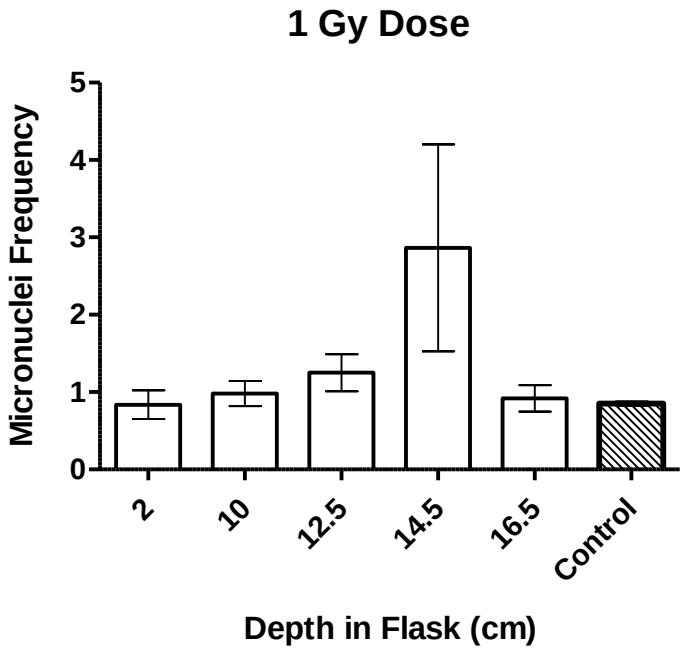

Figure 17. Micronuclei frequency at increasing depths in T-175 flasks. CBMN assays were conducted in Greiner T-175 cell culture flasks, following a 1-day incubation period of CHO cells irradiated with 290 MeV/n carbon-ions at an initial dosage of 1 Gy. Depths chosen to evaluate in correlation to survival assay depths portraying greatest differences in colony formation. Micronuclei frequency increased with an increased depth up to 14.5 cm. Micronuclei frequency was not found to be significant as compared to our control ($P = 0.2088$). Error bars indicate standard errors of the means from as many as three independent irradiation experiments as well as for our control.

2.4 Discussion

The main goal behind radiotherapy is to deprive cancer cells of being able to complete cell division, therefore the endpoint of cell survival is commonly used for *in-vitro* experiments [19]. Our new method for addressing cell survival allowed us to express the survival fraction at increasing depths in a single system following carbon-ion beam irradiation, in which the classical cell survival method could not. This method was important for more accurately determining the range of depths at which the dosages could be considered biologically lethal by portraying significant losses in cellular clonogenicity in our T-175 flasks.

The challenge with our new cell survival technique involved addressing which depths to evaluate to appropriately represent the monoenergetic 290 MeV/n carbon-ion beam dose distribution. The largest observable colonies were found to be approximately 0.4 cm. Thus, evaluation depths could not be less than 0.4 cm apart to insure no colonies would be incorporated at more than one of our depths. Under all irradiation initial dosages, we observed few to no colony formation at the depth of 14.5 cm in our T-175 flasks (Fig.12). Therefore, we determined this depth to be our biological Bragg peak and was important to incorporate into our evaluation depths. Moreover, a previous study utilizing the monoenergetic 290 MeV/n carbon-ion beam depicted large increases of dose beginning around the depth of ~10.0 cm in water [33]. Furthermore, observed color changes in our Fricke gel indicated an increase in dosage at depths of ~8.0 and ~12.5 cm, with the highest observed dose values ranging between the depths of ~13.8 - ~14.5 cm. Taken together, we chose to evaluate depths from beam entry up to the 10.0 cm in increments of 2.0 cm and from 10.0 to 18.0 cm in increments of 0.5 cm to incorporate our biological Bragg peak, as well as, to more precisely address the biological impacts surrounding this Bragg peak.

To further insure our evaluated depths depicted an accurate representation of survival fraction throughout our flasks we generated a surface plot for each of our experimental initial dosages (Fig.14). The advantage of this method was that it allowed for us to observe colony formation at all depths in our flask to ensure that there were no abnormal anomalies indicated outside of our evaluated depths. However, the disadvantage of this approach was that it could not decipher between surviving colonies vs non-surviving colonies, i.e. if the colony contained > 50 cells or not. Although, the results utilizing this technique were observed to be relatively consistent with our cell survival results, therefore supporting the accuracy of our chosen evaluated depths used for our cell survival assays.

In this study we observed a clear trend of decreasing survival fraction and increasing micronuclei formation as the depth increased up to the biological Bragg peak at 14.5 cm. However, our results were consistent with the carbon-ion displaying a sharp high dose Bragg peak [46]. Our CBMN assay results portrayed a relatively settle increase in MN formation between the depths of 2.0 and 10.0 cm with a higher increase in MN formation at 12.5 cm and the most notable increase occurring at the biological Bragg peak following a 1 Gy treatment dose (Fig.17). Moreover, at each increase of treatment dose the range of significant decrease in survival fractions increased as well ($P < 0.0001$), for the depths ranging between 14.0 – 14.5 cm, 13.5 – 14.5 cm and 12.5 – 14.5 cm for 1, 2 and 3 Gy, respectively (Fig.13A-C). These results suggest that as the initial dosage is increased the range of lethal dose distribution prior to the Bragg peak also increases.

Following our biological Bragg peak we expected the depth of colony reformation to remain consistent regardless of initial dosage, as previous studies have depicted there should be a steep drop-off of energy deposition [9, 33]. However, our results portrayed a significant increase

in the depth of reappearance of colony formation following the biological Bragg peak, as the initial dosage increased from 1 Gy to 3 Gy, this depth increased from 147.22 ± 0.4 mm to 147.89 ± 0.3 mm, respectively ($P < 0.05$) (Fig.16). In addition, we observed a higher number of MN at the depth of 16.5 cm compared to the depth of 2.0 cm. This result conflicted with of our cell survival assay depicting the highest survival fraction at the depth of 16.5 cm, indicating there should have been less MN at 16.5 cm than at 2.0 cm. Although, it is important to note that our control indicated that CHO cells possessed a relatively high level of background MN formation as the initial evaluated depth of 2.0 cm portrayed similar MN formation as with our control (Fig.17). Taken together, these results suggest that the carbon-ion fragmentation tail is capable of inducing genotoxicity and cell death. Therefore, the carbon-ion lethal dose range may extend past the biological Bragg peak depth as well.

Carbon-ion nuclear fragmentation may have also resulted in discrepancies involving the NIRS calculated Bragg peak vs. our biologically observed Bragg peak depth. Our dose-response curve portrayed a clear trend of decreasing cell survival as the dose increased for both LET < 50 keV/μm and LET > 50 keV/μm (Fig.15). However, our cell survival results were inconstant with the dose vs depth data provided from NIRS, particularly for depths ranging between 14.0 – 14.5 cm in our flasks (Tables.2-3). Their data suggested that their calculated Bragg peak was at 14.202 cm (LET = 337 keV/μm), in contrast to our biologically observed Bragg peak depth of 14.5 cm. However, it is possible that their calculated Bragg peak provided by NIRS may have been accurate, as our cell survival assay results portrayed significant decreases in colony formation ($P < 0.0001$) for the depths ranging between 14.0 – 14.5 cm under all our experimental initial treatment dosages (Fig.13A-C). Moreover, our Fricke gel indicated the highest observed dose values ranged between the depths of ~13.8 - ~14.5 cm (Fig.11), which

suggested that the Bragg peak did indeed fall between this range but did not provide us with an adequate determination of the precise depth of the Bragg peak in our flask. Therefore, if their calculated Bragg peak was accurate, it may further support that the carbon-ion fragmentation tail may be highly lethal and can induce its lethality over greater distances past the Bragg peak than previously anticipated.

A potential drawback of utilizing our new survival assay variation technique was that we could not use a cell line possessing large colony sizes in order to not incorporate a colony at more than one depth. Therefore, we used the CHO cell line, as no colonies were observed to be greater than 0.4 cm. However, this drawback became problematic for precisely determining the Bragg peak depth, as the calculated Bragg peak vs our biologically observed Bragg peak involved depths less than 0.5 cm apart. Another drawback of this study involved the determination of accurate dosages at each of our evaluated depths, as NIRS disclosed that data values possessing LET $\geq$ 70 keV/μm could not be guaranteed for the biological experiments. This may have been due to the dose calculation algorithm in which they used being simple and fast but lacks accuracy for highly heterogenous systems [78]. Furthermore, their planner-integrated dose was determined from the measured dose distribution with a large area parallel plate ionization chamber and data was fitted to a simple formula and incorporated into planning software. Moreover, the dose delivered to the target is reduced according to the field size in carbon-ion scanning with the thickness of their range shifter plates, which may have accounted for some of these discrepancies as the thickness of our flask at the beam entry site may have shifted our proposed biological Bragg peak depth [78].

In conclusion, our results suggest that monoenergetic 290 MeV/n carbon-ion beams portrayed a biologically observed Bragg peak at the depth of 14.5 cm in our flask. Furthermore,

that there is a range in which the carbon-ion beam distributed lethal dosage both prior to and following its Brag peak depth, which increased with an increased initial dosage. Moreover, our results suggested that nuclear fragmentation of the carbon-ion beam may be responsible for cell death and genotoxicity past the carbon-ion beam Bragg peak. By defining this biological lethal dosage range, it will aid physicians in accurately targeting tumor tissues while limiting the cell death in the surrounding normal tissues.

CHAPTER THREE

CONCLUSION AND FUTURE DIRECTIONS

Our *in-vitro* new cell survival method and CBMN assays portrays a more biologically representative assessment of the range in which carbon-ion irradiation induces cell death. This biological lethal dose range is of clinical importance as it will aid physicians in accurately targeting tumor tissues while limiting any unwanted cell death in the surrounding normal tissues. Our results indicated that monoenergetic 290 MeV/n carbon-ion beams for 1, 2 or 3 Gy initial dosages display a biological lethal dose range of 0.72, 1.27 and 2.28 cm, respectively. As we observed following 1, 2 or 3 Gy initial dosages, the survival fractions were most significantly reduced between the ranges of 14.0 – 14.5, 13.5 – 14.5 and 12.5 – 14.5 cm ($P < 0.0001$), as well as, reappearance of colony formation occurring at the depths of 14.72, 14.77 and 14.78 cm, respectively.

Discrepancies between the NIRS calculated Bragg peak depth of 14.202 cm vs our biologically observed Bragg peak depth of 14.5 cm, in which survival fraction was observed at its lowest and micronuclei formation was observed at its highest, represents an area for future studies. The most likely causality for these discrepancies may have been the result of nuclear fragmentation of the carbon-ion, resulting in unwanted cellular lethality upstream from the actual depth of the Bragg peak. It is of importance to further address this issue in future studies as it suggests carbon-ion nuclear fragmentation may induce cell death following the carbon-ion beam Bragg peak.

By comparing the results obtained in this study with different radiation techniques/modalities undergoing the same experimental evaluation methods will provide for a

more detailed understanding of the biological effects each of these techniques/modalities portray. It is of clinical importance to repeat these experiments utilizing the clinically relevant spread-out Bragg peak (SOBP) 290 MeV/n carbon-ion irradiation technique to address if the SOBP technique produces cellular lethality to the same degree as the monoenergetic carbon-ion beam, as well as, if this technique demonstrates the same nuclear fragmentation effects as observed in this study. If it is found that the SOBP technique is consistent with our observed results utilizing the monoenergetic carbon-ion beam, it would require modification in the dose calculation of therapy for physicians to address the nuclear fragmentation and avoid healthy tissue damage past the target tumor tissue. Furthermore, repeating these experiments with the proton beam will help specify the degree in which the carbon-ion beam provides a more precise distribution of biological lethal dosages, thus providing more support for the expansion of these facilities over the more common proton facilities used today.

Another important area for future studies would involve enhancing carbon-ion beams ability to induce cell death. As previously described in chapter 1, irradiation-induced DNA damage can result from the production of free radicals, i.e. indirect action. However, this type of irradiation-induced DNA damage is mostly contributed to low-LET radiations [35]. In contrast, high-LET carbon-ions mainly induce DNA damage directly, without the production of these free radicals [34]. Therefore, treatment with a transition metal, such as copper, may enhance the production of these free radicals following carbon-ion irradiation via the Fenton reaction. As a result, this may enhance the frequency in which there is DNA damage following irradiation, thus causing an increase in cell death. This would mean that lower dosages and less fractions may be needed to treat tumors, therefore decreasing the cost of undergoing carbon-ion radiotherapy as well as increasing the effectiveness to successfully “kill” the tumor.

REFERENCES

1. Fidler, M.M., et al., *Cancer incidence and mortality among young adults aged 20-39 years worldwide in 2012: a population-based study.* Lancet Oncol, 2017. **18**(12): p. 1579-1589.
2. Society, A.C., *Cancer Facts & Figures 2018.* Altlanta: American Cancer Society, 2018., 2018.
3. Fujisawa, H., et al., *Comparison of human chordoma cell-kill for 290 MeV/n carbon ions versus 70 MeV protons in vitro.* Radiat Oncol, 2013. **8**: p. 91.
4. Begg, A.C., F.A. Stewart, and C. Vens, *Strategies to improve radiotherapy with targeted drugs.* Nat Rev Cancer, 2011. **11**(4): p. 239-53.
5. Singleterry, J., *The Costs of Cancer.* American Cancer Society Cancer Action Network, 2017.
6. Coates, A., et al., *On the receiving end--patient perception of the side-effects of cancer chemotherapy.* Eur J Cancer Clin Oncol, 1983. **19**(2): p. 203-8.
7. Curigliano, G., et al., *Cardiac toxicity from systemic cancer therapy: a comprehensive review.* Prog Cardiovasc Dis, 2010. **53**(2): p. 94-104.
8. Monsuez, J.J., et al., *Cardiac side-effects of cancer chemotherapy.* Int J Cardiol, 2010. **144**(1): p. 3-15.
9. Baskar, R., et al., *Cancer and radiation therapy: current advances and future directions.* Int J Med Sci, 2012. **9**(3): p. 193-9.
10. Lengyel, E., et al., *Malignant mucosal melanoma of the head and neck.* Pathol Oncol Res, 2003. **9**(1): p. 7-12.
11. Mendenhall, W.M., et al., *Radiotherapy alone or combined with surgery for adenoid cystic carcinoma of the head and neck.* Head Neck, 2004. **26**(2): p. 154-62.
12. Lomax, A.J., *Charged particle therapy: the physics of interaction.* Cancer J, 2009. **15**(4): p. 285-91.
13. Jelena, Z., et al., *Carbon ions of different linear energy transfer (LET) values induce apoptosis & G2 cell cycle arrest in radio-resistant melanoma cells.* Indian J Med Res, 2016. **143**(Supplement): p. S120-S128.
14. Costes, S.V., et al., *Spatiotemporal characterization of ionizing radiation induced DNA damage foci and their relation to chromatin organization.* Mutat Res, 2010. **704**(1-3): p. 78-87.
15. Dokic, I., et al., *Next generation multi-scale biophysical characterization of high precision cancer particle radiotherapy using clinical proton, helium-, carbon- and oxygen ion beams.* Oncotarget, 2016. **7**(35): p. 56676-56689.
16. Jackson, S.P. and J. Bartek, *The DNA-damage response in human biology and disease.* Nature, 2009. **461**(7267): p. 1071-8.
17. Asaithamby, A., B. Hu, and D.J. Chen, *Unrepaired clustered DNA lesions induce chromosome breakage in human cells.* Proc Natl Acad Sci U S A, 2011. **108**(20): p. 8293-8.
18. Lobrich, M. and P.A. Jeggo, *The impact of a negligent G2/M checkpoint on genomic instability and cancer induction.* Nat Rev Cancer, 2007. **7**(11): p. 861-9.

19. Furusawa, Y., *Heavy-Ion Radiobiology*, in *Carbon-Ion Radiotherapy: Principles, Practices, and Treatment Planning*, H. Tsujii, et al., Editors. 2014, Springer Japan: Tokyo. p. 25-37.
20. Karger, C.P. and P. Peschke, *RBE and related modeling in carbon-ion therapy.* Physics in Medicine and Biology, 2018. **63**(1).
21. Polo, S.E. and S.P. Jackson, *Dynamics of DNA damage response proteins at DNA breaks: a focus on protein modifications.* Genes Dev, 2011. **25**(5): p. 409-33.
22. Verheij, M., *Clinical biomarkers and imaging for radiotherapy-induced cell death.* Cancer Metastasis Rev, 2008. **27**(3): p. 471-80.
23. Vakifahmetoglu, H., M. Olsson, and B. Zhivotovsky, *Death through a tragedy: mitotic catastrophe.* Cell Death Differ, 2008. **15**(7): p. 1153-62.
24. Cohen–Jonathan, E., E.J. Bernhard, and W.G. McKenna, *How does radiation kill cells?* Current Opinion in Chemical Biology, 1999. **3**(1): p. 77-83.
25. Ugo, A. and K. Gerhard, *Radiotherapy with beams of carbon ions.* Reports on Progress in Physics, 2005. **68**(8): p. 1861.
26. Schulz-Ertner, D. and H. Tsujii, *Particle radiation therapy using proton and heavier ion beams.* J Clin Oncol, 2007. **25**(8): p. 953-64.
27. Weber, U. and G. Kraft, *Comparison of carbon ions versus protons.* Cancer J, 2009. **15**(4): p. 325-32.
28. Blakely, E.A., et al., *Inactivation of human kidney cells by high-energy monoenergetic heavy-ion beams.* Radiat Res, 1979. **80**(1): p. 122-60.
29. Cox, R., et al., *Mutation and inactivation of mammalian cells by various ionising radiations.* Nature, 1977. **267**(5610): p. 425-7.
30. Tsujii, H., *History of Charged Particle Radiotherapy*, in *Carbon-Ion Radiotherapy: Principles, Practices, and Treatment Planning*, H. Tsujii, et al., Editors. 2014, Springer Japan: Tokyo. p. 3-10.
31. Ma, C.M. and R.L. Maughan, *Within the next decade conventional cyclotrons for proton radiotherapy will become obsolete and replaced by far less expensive machines using compact laser systems for the acceleration of the protons.* Med Phys, 2006. **33**(3): p. 571-3.
32. Paganetti, H., *Relative biological effectiveness (RBE) values for proton beam therapy. Variations as a function of biological endpoint, dose, and linear energy transfer.* Phys Med Biol, 2014. **59**(22): p. R419-72.
33. Genet, S.C., et al., *Comparison of cellular lethality in DNA repair-proficient or -deficient cell lines resulting from exposure to 70 MeV/n protons or 290 MeV/n carbon ions.* Oncol Rep, 2012. **28**(5): p. 1591-6.
34. Lomax, M.E., L.K. Folkes, and P. O'Neill, *Biological consequences of radiation-induced DNA damage: relevance to radiotherapy.* Clin Oncol (R Coll Radiol), 2013. **25**(10): p. 578-85.
35. Ward, J.F., *DNA damage produced by ionizing radiation in mammalian cells: identities, mechanisms of formation, and reparability.* Prog Nucleic Acid Res Mol Biol, 1988. **35**: p. 95-125.
36. Wallace, S.S., *Biological consequences of free radical-damaged DNA bases.* Free Radic Biol Med, 2002. **33**(1): p. 1-14.
37. Lederman, M., *The early history of radiotherapy: 1895-1939.* Int J Radiat Oncol Biol Phys, 1981. **7**(5): p. 639-48.

38. Slater, J.M., *From X-Rays to Ion Beams: A Short History of Radiation Therapy*, in *Ion Beam Therapy: Fundamentals, Technology, Clinical Applications*, U. Linz, Editor. 2012, Springer Berlin Heidelberg: Berlin, Heidelberg. p. 3-16.
39. Jones, B., R.G. Dale, and A. Carabe-Fernandez, *Charged particle therapy for cancer: the inheritance of the Cavendish scientists?* Appl Radiat Isot, 2009. **67**(3): p. 371-7.
40. Nikjoo, H., et al., *Quantitative modelling of DNA damage using Monte Carlo track structure method.* Radiat Environ Biophys, 1999. **38**(1): p. 31-8.
41. Nikjoo, H., et al., *Track structure in radiation biology: theory and applications.* International Journal of Radiation Biology, 1998. **73**(4): p. 355-364.
42. Vignard, J., G. Mirey, and B. Salles, *Ionizing-radiation induced DNA double-strand breaks: a direct and indirect lighting up.* Radiother Oncol, 2013. **108**(3): p. 362-9.
43. Masunaga, S. and K. Ono, *Significance of the response of quiescent cell populations within solid tumors in cancer therapy.* J Radiat Res, 2002. **43**(1): p. 11-25.
44. Pawlik, T.M. and K. Keyomarsi, *Role of cell cycle in mediating sensitivity to radiotherapy.* Int J Radiat Oncol Biol Phys, 2004. **59**(4): p. 928-42.
45. Suit, H., et al., *Proton vs carbon ion beams in the definitive radiation treatment of cancer patients.* Radiother Oncol, 2010. **95**(1): p. 3-22.
46. Mohamad, O., et al., *Carbon Ion Radiotherapy: A Review of Clinical Experiences and Preclinical Research, with an Emphasis on DNA Damage/Repair.* Cancers (Basel), 2017. **9**(6).
47. McDonald, M.W. and M.M. Fitzek, *Proton therapy.* Curr Probl Cancer, 2010. **34**(4): p. 257-96.
48. Mohan, R. and D. Grosshans, *Proton therapy - Present and future.* Adv Drug Deliv Rev, 2017. **109**: p. 26-44.
49. Kamada, T., *Overview of the Heavy-Ion Medical Accelerator in Chiba (HIMAC) Practices*, in *Carbon-Ion Radiotherapy: Principles, Practices, and Treatment Planning*, H. Tsujii, et al., Editors. 2014, Springer Japan: Tokyo. p. 17-22.
50. Overgaard, J., *The role of radiotherapy in recurrent and metastatic malignant melanoma: a clinical radiobiological study.* Int J Radiat Oncol Biol Phys, 1986. **12**(6): p. 867-72.
51. Ramaekers, B.L., et al., *Systematic review and meta-analysis of radiotherapy in various head and neck cancers: comparing photons, carbon-ions and protons.* Cancer Treat Rev, 2011. **37**(3): p. 185-201.
52. Bragg, W.H. and R. Kleeman, *On the ionization curves of radium.* Philosophical Magazine, 1904. **8**(43-48): p. 726-738.
53. Ando, K., et al., *Biological gain of carbon-ion radiotherapy for the early response of tumor growth delay and against early response of skin reaction in mice.* J Radiat Res, 2005. **46**(1): p. 51-7.
54. Kamada, T., *The Characteristics of Carbon-Ion Radiotherapy*, in *Carbon-Ion Radiotherapy: Principles, Practices, and Treatment Planning*, H. Tsujii, et al., Editors. 2014, Springer Japan: Tokyo. p. 13-16.
55. Haettner, E., et al., *Experimental study of nuclear fragmentation of 200 and 400 MeV/u (12)C ions in water for applications in particle therapy.* Phys Med Biol, 2013. **58**(23): p. 8265-79.
56. Iwata, Y., et al., *Development of Carbon-Ion Radiotherapy Facilities at NIRS.* Ieee Transactions on Applied Superconductivity, 2018. **28**(3).

57. Kamada, T., et al., *Carbon ion radiotherapy in Japan: an assessment of 20 years of clinical experience.* Lancet Oncol, 2015. **16**(2): p. e93-e100.
58. Niemantsverdriet, M., et al., *High and Low LET Radiation Differentially Induce Normal Tissue Damage Signals.* International Journal of Radiation Oncology Biology Physics, 2012. **83**(4): p. 1291-1297.
59. Goodhead, D.T., *Initial events in the cellular effects of ionizing radiations: clustered damage in DNA.* Int J Radiat Biol, 1994. **65**(1): p. 7-17.
60. Bird, R.P. and H.J. Burki, *Survival of synchronized Chinese hamster cells exposed to radiation of different linear-energy transfer.* Int J Radiat Biol Relat Stud Phys Chem Med, 1975. **27**(2): p. 105-20.
61. Fournier, C. and G. Taucher-Scholz, *Radiation induced cell cycle arrest: an overview of specific effects following high-LET exposure.* Radiother Oncol, 2004. **73 Suppl 2**: p. S119-22.
62. Wang, H., et al., *S-phase cells are more sensitive to high-linear energy transfer radiation.* Int J Radiat Oncol Biol Phys, 2009. **74**(4): p. 1236-41.
63. Ebner, D.K. and T. Kamada, *The Emerging Role of Carbon-Ion Radiotherapy.* Front Oncol, 2016. **6**: p. 140.
64. Tsujii, H., *Overview of Carbon-ion Radiotherapy*, in *Micro-Mini & Nano-Dosimetry & Innovative Technologies in Radiation Therapy*, C. Baldock, A. Rozenfeld, and P. Metcalfe, Editors. 2017.
65. Grassberger, C., et al., *Variations in linear energy transfer within clinical proton therapy fields and the potential for biological treatment planning.* Int J Radiat Oncol Biol Phys, 2011. **80**(5): p. 1559-66.
66. Streffer, C., W.-U. Müller, and K. Wuttke, *The Formation of Micronuclei after Exposure to Ionizing Radiation*, in *Chromosomal Alterations: Origin and Significance*, G. Obe and A.T. Natarajan, Editors. 1994, Springer Berlin Heidelberg: Berlin, Heidelberg. p. 214-222.
67. Jayapal, K.R., et al., *Recombinant protein therapeutics from CHO cells - 20 years and counting.* Chemical Engineering Progress, 2007. **103**(10): p. 40-47.
68. Tjio, J.H. and T.T. Puck, *Genetics of somatic mammalian cells. II. Chromosomal constitution of cells in tissue culture.* J Exp Med, 1958. **108**(2): p. 259-68.
69. Hall, E.J., *Radiobiology for the Radiologist: Cell survival curves*. 4th ed. 1994, Philidelphia: J.B. Lippincott Company.
70. Franken, N.A., et al., *Clonogenic assay of cells in vitro.* Nat Protoc, 2006. **1**(5): p. 2315-9.
71. Vral, A., M. Fenech, and H. Thierens, *The micronucleus assay as a biological dosimeter of in vivo ionising radiation exposure.* Mutagenesis, 2011. **26**(1): p. 11-17.
72. Geraud, G., et al., *Three-dimensional organization of micronuclei induced by colchicine in PtK1 cells.* Exp Cell Res, 1989. **181**(1): p. 27-39.
73. Fenech, M. and A.A. Morley, *Measurement of micronuclei in lymphocytes.* Mutat Res, 1985. **147**(1-2): p. 29-36.
74. Shibamoto, Y., et al., *Tumor radiosensitivity prediction by the cytokinesis-block micronucleus assay.* Radiat Res, 1991. **128**(3): p. 293-300.
75. Francis, Z., et al., *Carbon ion fragmentation effects on the nanometric level behind the Bragg peak depth.* Phys Med Biol, 2014. **59**(24): p. 7691-702.

76. Maeyama, T., et al., *Radiological properties of nanocomposite Fricke gel dosimeters for heavy ion beams.* J Radiat Res, 2016. **57**(3): p. 318-24.
77. Soliman, Y.S., et al., *Fricke gel dosimeter as a tool in quality assurance of the radiotherapy treatment plans.* Appl Radiat Isot, 2017. **120**: p. 126-132.
78. Kanematsu, N. and T. Inaniwa, *Treatment Planning of Carbon-Ion Radiotherapy*, in *Carbon-Ion Radiotherapy: Principles, Practices, and Treatment Planning*, H. Tsujii, et al., Editors. 2014, Springer Japan: Tokyo. p. 87-97.